



HAL
open science

Structural insights into serine-rich fimbriae from Gram-positive bacteria.

Stéphanie Ramboarina, James A Garnett, Meixian Zhou, Yuebin Li, Zhixiang Peng, Jonathan D Taylor, Wei-Chao Lee, Andrew Bodey, James W Murray, Yilmaz Alguel, et al.

► **To cite this version:**

Stéphanie Ramboarina, James A Garnett, Meixian Zhou, Yuebin Li, Zhixiang Peng, et al.. Structural insights into serine-rich fimbriae from Gram-positive bacteria.. *Journal of Biological Chemistry*, 2010, 285 (42), pp.32446-57. 10.1074/jbc.M110.128165 . pasteur-01500608

HAL Id: pasteur-01500608

<https://pasteur.hal.science/pasteur-01500608>

Submitted on 3 Apr 2017

HAL is a multi-disciplinary open access archive for the deposit and dissemination of scientific research documents, whether they are published or not. The documents may come from teaching and research institutions in France or abroad, or from public or private research centers.

L'archive ouverte pluridisciplinaire **HAL**, est destinée au dépôt et à la diffusion de documents scientifiques de niveau recherche, publiés ou non, émanant des établissements d'enseignement et de recherche français ou étrangers, des laboratoires publics ou privés.



Distributed under a Creative Commons Attribution - NonCommercial 4.0 International License

STRUCTURAL INSIGHTS INTO SERINE-RICH FIMBRIAE FROM GRAM-POSITIVE BACTERIA

Stéphanie Ramboarina^{1§*}, James A. Garnett^{1*}, Meixian Zhou², Yuebin Li², Zhixiang Peng², Jonathan D. Taylor¹, Wei-chao Lee¹, Andrew Bodey¹, James W. Murray¹, Yilmaz Alguel¹, Julien Bergeron^{1,3}, Benjamin Bardiaux⁴, Elizabeth Sawyer¹, Rivka Isaacson¹, Camille Tagliaferri¹, Ernesto Cota¹, Michael Nilges⁵, Peter Simpson¹, and Teresa Ruiz⁶, Hui Wu^{2#} and Stephen Matthews^{1#}

¹*Department of Biological Sciences, Centre for Structural Biology, Imperial College London, South Kensington, London SW7 2AZ, UK.*

²*Department of Pediatric Dentistry, University of Alabama at Birmingham, SDB 802, 1919 7th Avenue South, Birmingham, AL 35294-0007, USA*

³*Department of Infectious Diseases, King's College London School of Medicine, London, SE1 9RT, United Kingdom*

⁴*Structural Biology Unit, Leibniz Institute for Molecular Pharmacology, FMP Robert-Rossle –Str. 10, 13125 Berlin, Germany.*

⁵*Institut Pasteur Unité de Bioinformatique Structurale, 25-28 rue du Dr Roux, F-75724 Paris CEDEX 15, France*

⁶*Molecular Physiology and Biophysics, University of Vermont, Burlington, VT 05405, USA*

[§] *Present address: Department of Molecular and Cellular Interactions, VIB Structural Biology Brussels, Vrije Universiteit Brussel, Pleinlaan 2, B-1050 Brussels, Belgium.*

*These authors contributed equally; #Corresponding authors - SM (s.j.matthews@imperial.ac.uk) and HW(hwu@uab.edu)

The serine-rich repeat (SRR) family of fimbriae play important roles in the pathogenesis of streptococci and staphylococci. Despite recent attention, their finer structural details and precise adhesion mechanisms have yet to be determined. Fap1 (Fimbriae associated protein 1) is the major structural subunit of SRR fimbriae from *Streptococcus parasanguinis*, and plays an essential role in fimbrial biogenesis, adhesion and the early stages of dental plaque formation. Combining multidisciplinary, high resolution structural studies with biological assays we provide new structural insight into adhesion by Fap1. We propose a model in which the serine-rich repeats of Fap1 subunits form an extended structure that projects the N-terminal globular domains away from the bacterial surface for adhesion to the salivary pellicle. We also uncover a novel pH-dependent conformational change that modulates adhesion and likely plays a role in survival in acidic environments.

Biofilms offer protection to bacteria from hostile environments, such as adverse temperatures, pH and attack by other organisms including their hosts (1). Significant progress has been made toward understanding which gene products are involved in biofilm formation. Fimbriae, which are long, thin filamentous structures that decorate bacterial surfaces, are often employed in the reversible adhesion to surfaces at the early stages of biofilm formation (2). A large number of chronic bacterial infections involve the formation of a biofilm, with the development of dental plaque being one of the most familiar and diverse (3).

The commensal streptococci of the oral cavity play a major role in the foundation of dental plaque (4). These include early colonizers of the tooth surface, viridans *Streptococcus sanguinis* and *Streptococcus parasanguinis*, which serve as substratum for the subsequent adhesion of other microflora, such as cariogenic *Streptococcus mutans*, and periodontal pathogens *Porphyromonas gingivalis* and

Aggregatibacter actinomycetcomitans (5). In addition, both *S. sanguinis* and *S. parasanguinis* have been described as etiological agents in infective endocarditis (6-10) with the formation of streptococcal biofilms being central to the development of disease. Fap1 (Fimbriae associated protein 1) has been identified as the major structural subunit of *S. parasanguinis* fimbriae and is essential for fimbrial biogenesis, adhesion and biofilm formation (11-15). Fap1-like subunits assemble into a new family of fimbriae in Gram-positive bacteria (16), which are characterised by large polypeptides (>200 kDa) comprising an extensive region of glycosylated, serine-rich repeats (SRR) flanked by a unique N-terminal region and a C-terminal cell wall-anchoring domain. The SRR family of fimbriae play direct roles in several bacterial diseases; including the pathogenesis of streptococcal (17) and staphylococcal infective endocarditis (18), streptococcal meningitis (19), invasive pneumococcal disease (20) and neonatal disease (21-22).

Fap1 from *S. parasanguinis* provides a model system to study bacterial adhesion and biofilm formation by this poorly understood family of proteins. Furthermore, these adhesins play a major role in early stages of dental plaque formation. Despite recent attention, the finer structural details of SRR fimbriae and their adhesion mechanisms have yet to be determined. Combining multidisciplinary, high resolution structural studies with biological assays we provide new insights into adhesion by Fap1. We propose a model in which the serine-rich repeats of Fap1 subunits form an extended structure that projects the N-terminal globular domains away from the bacterial surface for adhesion to the salivary pellicle. We also uncover a novel pH-dependent conformational change that modulates adhesion and likely plays a role in survival in acidic environments.

Experimental procedures

Protein preparation- Recombinant Fap1-

NR (residues 106-437), Fap1-NR α (116-231) and Fap1-NR β (231-437) were expressed using pRSETA plasmid (Promega) in the BL21(DE3) *E. coli* strain (Novagen). Unlabelled proteins were produced in LB media whilst isotopically ^{15}N and ^{13}C -labelled proteins were produced in M9 minimal medium supplemented with $^{15}\text{NH}_4\text{Cl}$ and ^{13}C -glucose. A $^2\text{H}/^{15}\text{N}/^{13}\text{C}$ triple labelled Fap1-NR sample was produced from Silantes media in *E. coli* CDN OD1. Se-Met labelled Fap1-NR protein was expressed in methionine auxotroph B834 grown in minimal media supplemented with selenomethionine. All samples were purified using nickel affinity chromatography followed by size exclusion chromatography on a Superdex-75 column (GE healthcare). NMR samples were concentrated to 0.1-0.2 mM in 50 mM PBS, pH 8, 50 mM NaCl. X-ray diffraction samples were concentrated to ~8 mg/ml and stored at -72°C in 20 mM Tris-HCl pH 7.5, 100 mM KCl. SAXS samples were gel filtered in 50 mM PBS pH 5 or pH 8, 50 mM NaCl immediately prior to data collection.

NMR spectroscopy- NMR measurements were performed at 303K on [^{15}N , ^{13}C] labelled Fap1-NR α and Fap1-NR β domain samples in 50 mM PBS buffer, pH 8.0, 50 mM NaCl. NMR experiments for backbone and side-chain assignment on Fap1-NR α were performed on two different Bruker spectrometers, a DRX500 and an Avance II 800 equipped with cryoprobe. Assignments were completed using standard triple-resonance assignment methodology (23). NOE data for structure calculations of Fap1-NR α were obtained from an 800 MHz edited ^1H - ^{15}N nuclear Overhauser effect spectroscopy-heteronuclear single quantum coherence (NOESY-HSQC) and a 950 MHz edited ^1H - ^{13}C NOESY-HSQC experiments with a mixing time of 100 ms recorded on a 950 MHz Oxford superconducting magnet. ^{15}N T_1 and T_2 relaxation times on ^{15}N -labelled Fap1-NR α sample at pH 8 were recorded at 800 MHz and T_1/T_2 ratio measured for each residue.

^1H - ^{15}N and $^1\text{H}^\alpha$ - C^α residual dipolar coupling constants were measured using 2D in-phase anti-phase (IPAP)- ^{15}N - ^1H HSQC (24) and 3D HN(CO)CA experiments respectively on ^{15}N , ^{13}C labelled Fap1-NR $_\alpha$ sample at pH 8 partially aligned in Pf1 filamentous phage media. ^{15}N - ^1H TROSY-HSQC spectra of ^{15}N - ^2H Fap1-NR were recorded at pH 5, 6 and 8 at 800 MHz. A series of ^{15}N - ^1H HSQC on Fap1-NR $_\alpha$ at different pHs from pH 5 to pH 8 were performed at 500 MHz and 950 MHz. ^{15}N - ^1H HSQC on Fap1-NR $_\beta$ domain was performed at 800 MHz.

^1H - ^{15}N TROSY NMR experiments (25) were performed at 303K on a uniformly ^{15}N , ^{13}C , ^2H labelled Fap1-NR on a Bruker Avance II 800 equipped with a cryoprobe. TROSY versions of HNCACB, HN(CO)CACB experiments for backbone assignment allowed to assign ~50% assignment of Fap1-NR spectra. All NMR data were processed using NMRpipe (26) and analyzed with NMRView (27).

NMR structure determination- The ARIA protocol for automated NOESY assignment interfaced with the CNS program was used for structure calculation (28-30). Secondary helical structure in Fap1-NR $_\alpha$ was first identified using the chemical shift-based dihedral angle prediction software TALOS (31). For residues located in helices, hydrogen bonds, ϕ and ψ backbone dihedral angles derived from TALOS and RDCs were introduced as restraints in the ARIA structure calculation. 38 D_{NH} and 54 $D_{\text{C}\alpha\text{H}\alpha}$ RDCs spread evenly among the three helices were used for structure calculation. Axial D_a and rhombic R components were initially estimated using the histogram method from the normalized distribution of these 92 RDCs (32). The axial ($D_a = -3.0$ Hz) and rhombic ($R = 0.55$) components of the alignment tensor were further optimized with the program MODULE (33) based on the precalculated structures. For NOE derived and hydrogen bonds distances restraints, a log-harmonic potential was used for the second Cartesian cooling phase of the

simulated annealing and the weight on the restraints was iteratively updated (34). The final average weights were 6.8 kcal/mol/Å² for NOE restraints and 25 kcal/mol/Å² for hydrogen bonds restraints. To avoid distortion of the peptide group during Cartesian cooling, high force constants were used to maintain planarity, while low force constants were employed for RDC restraints. Furthermore, the final structures were carefully inspected for local distortions. 100 conformers were calculated in the final iteration and 10 lowest energy structures were refined in a shell of water molecules (35). A summary of NMR-derived restraints and statistics on the ensemble of NMR structure is reported in Table 2. The solution structure of the Fap1-NR $_\alpha$ domain was deposited in the Protein Data Bank with PDB ID code 2kub.

Crystallisation, data collection and structure determination- Crystals of both native and Se-Met labelled Fap1-NR were grown at 297K using the hanging drop vapour diffusion method in 0.1 M Hepes over a range of pH from pH 6.5 to 8.0, 5% MPD, 10-12.5% PEG 6K and 9-12.5 mM spermine-tetra HCl. Crystals were briefly soaked in the mother liquor supplemented with 20% PEG 6K before cryocooling. SeMet labelled Fap1-NR data were collected at the selenium peak energy, determined by a fluorescence scan, at beamline ID29 at the European Synchrotron Radiation Facility (ESRF) in Grenoble, France. Data were processed using MOSFLM and scaled with SCALA (36). Two selenium sites were located using SHELXD (37), and then phases were calculated using AUTO-SHARP. Two monomers were located in the electron density, and a model was built into the averaged solvent flattened experimental map using COOT (38), with rounds of refinement in REFMAC5 (39). The final model was refined with NCS restraints and TLS groups, with 5% of the reflections omitted for cross-validation. Statistics of data collection and the final model are shown in Table 1. The coordinates and

structure factors have been deposited in the PDB under accession code 2x12.

Small angle X-ray scattering (SAXS)- SAXS data were recorded at the X33 beamline of EMBL (DESY, Hamburg). Samples of Fap1-NR buffered at either pH 5 or pH 8 and at 1.3, 2.7 and 4.5 mg/ml were measured using 120 s exposures to synchrotron radiation. The range of q values measured was from 0.07 to 0.48 Å⁻¹. SAXS data were processed in the standard manner using the program PRIMUS (40). Data points across all three concentrations were merged (points 1-300, 250-600, and 550-2000 were derived from the low, medium and high concentration samples, respectively). The radius of gyration, R_g , and scattering at zero angle, $I(0)$, were calculated from the analysis of the Guinier region by AUTORG. The distance distribution function, $P(r)$, was subsequently obtained using GNOM, yielding the maximum particle dimension, D_{max} . An ensemble of 20 low-resolution *ab initio* structures were calculated using the program GASBOR utilising default parameters (41). Models were then aligned and averaged by DAMAVER. The known atomic resolution structures of the α and β domains were docked into the low-resolution bead model of Fap1-NR at pH 8 by the program SITUS (42). This was achieved by splitting the bead model into two halves and independently minimising the fit between the high- and low-resolution structures.

Site-directed mutagenesis of Fap1 of S. Parasanguinis- Surface regions containing an abundance of exposed hydrophobic amino acid side chains were selected for mutation. The hydrophobic residues together with selected hydrophilic side chains were mutated individually to alanine using the Stratagene quick change mutagenesis system as previously described (43). This included I134, E138, D142, L163 and V164 in Fap1-NR $_{\alpha}$ together with L385, I291, L292, L300, N403, Q405 and I411 in Fap1-NR $_{\beta}$. In brief, the full-length *fap1* gene cloned into an *E. coli* and Streptococcal

shuttle vector pVA838 was used as a template. Site-directed mutagenesis PCR was carried out to construct a series of alanine replacement mutants of *fap1* using the mutagenic oligonucleotide primers that corresponded to the changes of selected amino acid residues to alanine residues. The amplified mutant plasmids were transformed into competent *E. coli* following the instructions by a QuickChange XL Mutagenesis kit (Stratagene, La Jolla, CA). The plasmids with designed mutations were purified; the mutated region was sequenced to ensure the accuracy of the site-directed mutagenesis. The wild type and mutant plasmids were then transformed into a *fap1* mutant of *S. parasanguinis*. Fap1 expression was monitored by Western blot analysis using an antibody against mature Fap1 (F51).

Adhesion of S. parasanguinis to SHA: an in vitro tooth model- Adhesion of *S. parasanguinis* to saliva-coated hydroxylapatite (SHA) was performed as described previously (11). In brief, cells of wild type *S. parasanguinis* and site-directed mutants were labeled with 2 μ Ci of [*methyl*-³H]thymidine/ml. The radiolabeled bacteria were incubated with SHA beads at 37°C for 1 hr to allow bacterial binding to occur and then washed. Supernatants and washed beads were transferred to scintillation vials, and their respective radioactivities were determined and used to calculate adhesion percentage as previously described. In all assays a wild-type strain FW213 and the *fap1*-minus mutant were used as positive and negative controls, respectively.

Adhesion blocking assays- Wild type *S. parasanguinis* cells were labeled with 2 μ Ci of [³H]thymidine/ml. The radiolabeled cells were treated and reconstituted as previously described. Recombinant Fap1-NR, Fap1-NR $_{\alpha}$ and Fap1-NR $_{\beta}$ were expressed and purified as described. The purified recombinant proteins were dialyzed overnight against the adhesion buffer and added into SHA beads which were

equilibrated with adhesion buffer and then incubated at 37°C for 1 h on a rotating shaker. The treated SHAs were incubated with labeled *S. parasanguinis* and subjected to the adhesion assay described above.

Electron microscopy- *S. parasanguinis* (FW213) was grown from frozen stocks preserved with 5% dimethylsulfoxide (44). Frozen cells were streaked onto blood agar plates, and incubated aerobically for 12-15 h in 5% CO₂ at 37°C. Broth cultures were prepared by inoculation of single colonies from the blood agar plates into flasks containing Todd-Hewitt Broth (THB) and grown statically under aerobic conditions. 5 ml cell cultures in early exponential phase (A470~0.4) were centrifuged at 4000 g to remove the media. Cell pellets were resuspended in 100 µl PBS (100 mM Phosphate buffer pH 7.4, 150 mM NaCl) at 4°C.

Samples were diluted in PBS to the appropriate concentration for electron microscopy studies. A small aliquot (5µl) was applied to 400 mesh copper grids coated with a thin carbon film. The grids were washed by running several drops of PBS buffer over them and negatively stained by subsequently running a few drops of the staining solution (1% uranyl acetate (UA; Ted Pella, USA), 2% phosphotungstic acid, pH 7 with NaOH (PTA; Ted Pella, USA) and 2% methyl amine tungstate (MAT, Nanoprobes, USA) over the grids. The last drop of stain was left on the grid for 30 s; the excess liquid was wicked off, and the grids were fast air dried. The grids were observed using a dual-axis tomography holder (Fischione, USA) on a Tecnai 12 electron microscope (FEI, USA) equipped with an LaB6 cathode (Kimball, USA) operated in point mode, and a 14 µm 2048*2048 CCD camera (TVIPS, Germany). The microscope was run under identical conditions as have been used in the past to obtain images that show Thon rings beyond 0.9 nm resolution in vitreous ice preparations (45). Negatives were recorded at an accelerating voltage of 100 kV and nominal magnification of

52000X under low dose conditions on S0-163 Kodak film (~ 1000e-/nm²). Negatives were scanned with 7µm raster size on a Zeiss flat bed scanner (Intergraph, USA). The images were converted for processing with the SPIDER image processing system (46) and reduced two times to a final pixel size of 0.27 nm at the specimen level. A contrast transfer function correction was performed on the images by calculating the averaged periodogram of each image and fitting to it the theoretical transfer function calculated by varying the defocus value and astigmatism parameters (angle and strength) (47). Each image was corrected by multiplying it with a modified version of its transfer function (47).

Straight filament regions, which showed no overlap were boxed with the program 'heliboxer' in the EMAN image processing package (48). Images containing 55 nm filament sections were windowed using the SPIDER image processing system (46). The unevenness of the background was removed using the 'ramp' command and the intensities were normalized to zero average (5 pixels strips along the longitudinal edge of the images were used to calculate the average intensity value of the background). A power spectrum was calculated from each image and an averaged power spectrum was calculated for each stain condition. The averaged power spectra were visualized using the WEB display program (46) and the height of the layer lines was extracted.

RESULTS

Major non-repeat region of Fap1 blocks S. parasanguinis adhesion to SHA. Recently, SRR fimbrial proteins known to interact with salivary components and human platelets have also been identified in other medically-relevant streptococcal and staphylococcal species (49). Interestingly, the sequences of regions outside the serine-repeats are implicated in adhesion and poorly conserved amongst the family (50-53). To define the minimal region responsible for Fap1 adhesion to the salivary pellicle, the non-

repeat portion from the N-terminus of Fap1 (Fap1-NR, residues 106-437; Fig. 1A) was recombinantly produced in *E. coli*, purified using metal affinity chromatography and tested for its ability to inhibit *S. parasanguinis* adhesion to an *in vitro* tooth model, saliva-coated hydroxyapatite (SHA). Binding assays revealed a dose-dependent decrease in binding in the presence of recombinant Fap1-NR indicating that this region of Fap1 is able to competitively block adhesion (Fig. 1B).

Limited trypsin proteolysis of Fap1-NR released two stable domains corresponding to a C-terminal 25 kDa polypeptide and a smaller 10 kDa N-terminal fragment, confirmed by mass spectrometry (data not shown). To investigate the contribution of these sub-domains to adhesion, we produced Fap1-NR_α and Fap1-NR_β separately in *E. coli* and tested their ability to block *S. parasanguinis* binding to SHA (Fig. 1B). Each domain shows a dose dependent reduction in *S. parasanguinis* adhesion suggesting that they both play important roles in adhesion.

Structure of the major non-repeat region Fap1-NR. To explore the potential cooperative roles of Fap1-NR_α and Fap1-NR_β, and provide a better understanding of adhesion by Fap1, we embarked on a high-resolution structural investigation. We initiated our structural studies using the intact 36 kDa Fap1-NR. Crystals of Fap1-NR were obtained after one day, between pH 6.5 and pH 8.5, with the highest resolution diffraction obtained for crystals grown at pH 8. Structure determination was undertaken using Se-SAD and the electron density map was refined to 2.9 Å (Table 1 and Supplementary Fig. S1). The β-domain was built into the experimental electron density map from residue T236 to D435, while the electron density corresponding to all preceding residues was not observable. Crystals were washed and analysed by SDS-PAGE, which showed no sign of degradation (data not shown), therefore it was postulated that the lack of electron density for this

portion of Fap1-NR results from significant disorder in the N-terminal region, which encompasses Fap1-NR_α. The final model contains two identical molecules of the β-domain in a head to tail arrangement within the asymmetric unit. The dimer interface is small, comprising only the short loop connecting β10 and β11 in the monomer structure (Fig. 2A), which implies that dimer formation is most likely an artefact of crystal packing. Gel filtration experiments also indicate that, under these conditions Fap1-NR is largely monomeric in solution (Supplementary Fig. S2). The β-domain is composed of 12 β-strands arranged in two extensive β-sheets built from four anti-parallel β-strands (Figs. 2A, B). Four additional, short β-strands elaborate one face of the structure, creating an extended twisted β-platform. A striking feature is the presence of large loops protruding at the top (L1-L2-L5) and the bottom (L3-L6-L9) of the β-sandwich, and obscuring the face of the extended β-sheet (L4-L7-L8; Figs. 2A, B). These loops are well-ordered and are stabilized through hydrophobic interactions with exposed aromatic residues from the β-sheet core structure. A series of hydrophobic residues within L1-L2-L5 form an exposed ledge on the top of the structure (Supplementary Fig. S3).

The absence of electron density for the N-terminus of Fap1-NR_α may be due to lack of structural integrity or the presence of multiple, but ordered, conformations, arising from flexibility within the 27 amino acid linker. To elucidate the structure of this domain we used solution-state nuclear magnetic resonance (NMR) spectroscopy. 2D ¹H-¹⁵N HSQC spectra displays excellent dispersion in backbone amide chemical shifts at pH 8, consistent with a folded polypeptide (Supplementary Fig. S4). The ¹⁵N relaxation rates at pH 8 for backbone amides between E128 and L208 reveal a well ordered structure with no flexible loops or residues in chemical exchange, while the termini (residues 116-127 and 209-231) are highly flexible. Furthermore, NMR spectra indicate that Fap1-NR_α is monomeric at

concentrations up to 300 μM , but self-associates at higher concentrations (Supplementary Fig. S5).

Using a combination of manual and ARIA NMR assignment methods for Fap1-NR $_{\alpha}$ (28-29), a total of 1586 nuclear Overhauser effects (NOEs) were assigned in Fap1-NR $_{\alpha}$ $^{15}\text{N}/^{13}\text{C}$ -edited NOESY spectra at pH 8. The structure determination was supplemented with ϕ and φ dihedral angles and 92 residual dipolar coupling restraints (Table 2). All areas of secondary structure are well defined (Fig. 2C); the average pairwise root mean squared deviation (RMSD) for the water-refined final structures is 0.39 ± 0.06 Å for the backbone atoms and 0.81 ± 0.07 Å for the heavy atoms of residues within secondary structure. The final structure of the Fap1-NR $_{\alpha}$ exhibits an α -helical bundle topology (Fig. 2C), in which the three α -helices pack against each other in an up-down-up arrangement ($\alpha 1$ residues 129 to 150, $\alpha 2$ residues 153 to 178 and $\alpha 3$ residues 184 to 206). Hydrophobic interactions involving the side-chains of leucine, alanine and isoleucine residues stabilize the inter-helix interactions (Fig. 2D). The comparison of the ^{15}N - ^1H TROSY HSQC of Fap1-NR with spectra of both isolated Fap1-NR $_{\alpha}$ and Fap1-NR $_{\beta}$ indicates that while the majority of peaks for each isolated domain superimpose well with the corresponding peaks in Fap1-NR and a limited number of peaks exhibit chemical shifts differences, indicating the presence of a small interface between the domains (Supplementary Fig. S4). Furthermore, differences in ^{15}N relaxation times for α and β domains within Fap1-NR indicate some interdomain flexibility (Average T_1/T_2 ratios are 21 and 27 for α and β domains respectively; Supplementary Figure S5).

pH-dependent conformation change within Fap1. The oral cavity experiences a wide pH range, from neutrality at the normal saliva buffering conditions to values below 5.0, induced by the fermentation of ingested sugars by resident bacteria. To investigate the effect of pH on *S. parasanguinis*

adhesion, SHA-binding assays were repeated over a range of pH values. A progressive increase in adhesion was observed as the pH was lowered from alkaline (pH 8) to acidic (pH 5) conditions (Fig. 3A), whereas no change in basal adhesion for the *fap1* mutant strain was observed (Supplementary Fig. S6). To characterise this further 2D ^1H - ^{15}N TROSY-HSQC spectra of Fap1-NR were recorded over the same pH range (Supplementary Fig. S7). Intriguingly, strong pH dependences were observed for many ^1H and ^{15}N chemical shifts of residues located within the α -domain, while the majority of the residues from the β -domain were not affected (Supplementary Data S7). CD experiments performed between pH 5 and pH 8 indicate that the α -helical content remains unchanged over the pH range (data not shown). This was confirmed by repeating the pH titration and monitoring ^1H and ^{15}N chemical shifts of amides within the isolated Fap1-NR $_{\alpha}$ domain (Fig. 3B). After reassignment of the NMR spectra at pH 5, an analysis of backbone secondary shifts indicates that the three α -helices remain largely intact, consistent with CD measurements, and that no unfolding occurs between the pH 8 and pH 5. Amide chemical shift changes are localised to one end of the α -helical bundle (Fig. 3C,D). Although no histidine residues are present, the Fap1-NR $_{\alpha}$ domain possesses eighteen charged residues (twelve acidic and six basic; Supplementary Data S8). Interestingly, the amide resonances for three of these residues (R146, D152, E154 and K207) titrate with pH. Furthermore, chemical shift changes of several hydrophobic residues (L148, L151, L157, A165, I206 and L208) proximal to charged groups are also observed. (Supplementary Data S8). Decreasing the pH may cause a rearrangement of the relative orientation and/or dynamics of the α -helices.

Small angle X-ray scattering (SAXS) provides useful low resolution information on the global structural features of proteins in solution. This technique is sensitive to changes in relative position of domains or

positions of secondary structure and is therefore highly suitable for determining the overall structure of Fap1-NR under acidic and alkaline conditions. After exhaustive gel filtration chromatography of recombinant Fap1-NR at pH 8 and pH 5, SAXS measurements were recorded (Figs. 4A and 4B; Table 3). The resulting SAXS density indicates that Fap1-NR exists as a curved, extended structure comprising two domains (Fig. 4B). The relative sizes of Fap1-NR $_{\alpha}$ and Fap1-NR $_{\beta}$ domains are consistent with two halves of the density. Comparison of the data at pH 8 and pH 5 reveals a subtle difference in conformation, as judged by a change in the shape of the pair-distance distribution function (Fig. 4A). Upon reducing the pH the pair-distance distribution shifts to longer distances, for which a plausible interpretation would be an opening of the two domain structure (Fig. 4C). It is also likely that the extent of interdomain mobility is affected by pH and would contribute to an altered SAXS profile. It is interesting to note that the residues affected by the change in pH within the α -domain would be situated adjacent to the 27 residue linker between Fap1-NR $_{\alpha}$ and Fap1-NR $_{\beta}$ (Fig. 4D).

Analysis of the atomic resolution details of Fap1-NR reveals two patches on the surfaces of the α - and β -domains that comprise a number of exposed hydrophobic side chains (Fig. 4D). The exposed hydrophobic residues together with selected adjacent residues within these regions were selected for mutation; including 5 amino acids in Fap1-NR $_{\alpha}$ (I134, E138, D142, L163 and V164) and 7 amino acids located within the hydrophobic patch within L1-L2 and L5 in Fap1-NR $_{\beta}$ (L385, I291, L292, L300, N403, Q405 and I411) (Fig. 2A,B; Fig 4D and Fig. S3). We hypothesized that these residues may form part of a binding site for the salivary pellicle and created a series of site-specific Fap1 mutants in this region within *S. parasanguinis* and measured their ability to adhere to SHA (Fig. 4E). As a control a charge mutation at Fap1-E204A on the opposite face of the α -domain was also

constructed and tested. Western blot analysis revealed that all the mutants expressed Fap1 (data not shown), however all exhibited deficiencies in bacterial adhesion with the exception E204A.

Overall structure of Fap1. We analyzed the feasibility of imaging the fimbriae on the bacterial surface of the wild-type strain (FW213) for structure determination by single particle electron microscopy using several negatively stained preparations. Good results were obtained with preparations in 1% uranyl acetate (UA), 2% phosphotungstic acid, pH 7 (PTA) and 2% methyl amine tungstate (MAT) (Fig. 5A). The fimbriae are very flexible structures that bend easily in all the preparations. A close look at individual fimbriae reveals a diameter of \sim 5.5 nm and an internal substructure with a periodicity of \sim 6.5 nm. At neutral pH, fimbriae are close together forming rafts and the internal substructure is more apparent (Fig. 5A, open white arrows). At low pH (UA staining), the tip of the fimbriae come together to form aggregates (Fig. 5A, white arrows), in which the adhesion points are located uniquely at the tip of the fimbriae. Strikingly, despite the fimbriae being more abundant on the cell surface at pH 7.0 using staining reagents PTA and MAT, the tips do not come together. Even though an additional contribution from the electrostatic charges of the different stains at the experimental pH cannot be ruled out at the present time, these data support the notion of a pH-dependent conformational change for Fap1.

Once electron micrographs of whole-mount bacterial preparations in different negative stains had been collected, digitized, and corrected for the contrast transfer function (CTF) of the microscope, fimbrial regions were extracted from the images following strict criteria: the fimbriae should be straight; they should not overlap other fimbriae and they should be separated by at least two fimbrial diameters from its nearest neighbor (Fig. 5B). As many images as possible, with a length of \sim 55 nm, were

extracted from the boxed fimbrial regions. After centering the images, an average image (Fig. 5B) and an average power spectrum (Fig. 5C) were calculated for each staining condition. The power spectra, in all stain preparations, show predominant layer-lines at $1/(6.5 \text{ nm})$ and $1/(33 \text{ nm})$, which relate to structural repeats in the fimbriae. At the present time, an unambiguous assignment of the Bessel orders is not possible due to the weak scattering power of the fimbrial regions and the uncertainty in the diameter of fimbriae.

DISCUSSION

Recent studies have suggested that Fap1 belongs to a wider family of cell wall-anchored, serine-rich repeat proteins (49) that exhibit features distinct from the pili of other Gram-positive organisms, such as *Corynebacteria diphteria*, group A and group B *Streptococcus* (GAS and GBS) and Gram-negative bacteria expressing chaperone usher (CU) and Type IV secretion systems. Typically, these pili are characterised by small subunits non-covalently or covalently linked to each other (54-56), whereas SRR fimbriae are characterised by the presence of extensive glycosylated serine-rich repeats within a large protein subunit (>200 kDa). SSR fimbriae are found on several pathogenic streptococci and staphylococci, which include GspB from *Streptococcus gordonii* (17), SSR-1 and SSR-2 from *Streptococcus agalactiae* (21-22,57), SrpA from *S. sanguinis* (50) and SraP from *Staphylococcus aureus* (18). Many of these proteins mediate specific interactions with human platelets through their N-terminal regions, which share little sequence homology to each other and are implicated in binding to a diverse array of host receptors (20,57).

We have demonstrated that a 36 kDa fragment from the non-repeat region of Fap1 (Fap1-NR) harbours the binding properties for colonisation of the oral cavity (58). Fap1-NR comprises two domains with

distinct secondary structure and topology, namely an α -helical domain (residues 116-231, Fap1-NR $_{\alpha}$; Fig. 1A) and another composed predominantly of β -strands (residues 231-437, Fap1-NR $_{\beta}$; Fig. 1A). The protein sequence outside the non-repeat region is composed of ~2000 amino acid residues of S(V/I/E) dipeptide repeats. Perfect sequence repeats of less than four amino acids tend to form fibrous extended structures that are often super-helical (59); for example the collagen triple helix (60) and the zigzag beta structure of the silk I (61-62) and the β -turn helix of the *Plasmodium falciparum* circumsporozoite protein (63-64). The extensive repetition of the serine dipeptides together with our electron microscopy data suggests a model for the fimbriae in which Fap1 strands form a super-helical extended structure with a principal repeat at 6.5 nm and serine side-chains exposed for O-glycosylation (Fig. 6). The larger 33 nm periodicity may be attributed to an independent helical stripe of surface glycosylation, the exact pattern of which has yet to be determined. Furthermore, since there is an ambiguity in layer line indexing, fimbriae comprising a coiled coil arrangement of two or more Fap1 helical strands cannot be excluded. Fap1 fimbriae are variable in length (in 300-600 μm range), similar to other SRR fibrils e.g. SrpA on the surface of *S. cristatus* (65). These length variations could be attributed to more than one subunit present per fimbriae, linked in a head-to-tail fashion. Although the classic pilin motif for head-to-tail cross-linking is absent (56,66); lysines residues present at the N-terminus of Fap1 could act as substrates for this crosslinkage.

In this model the N-terminal non-repeat domain, Fap1-NR, comprises two globular domains that are located at the distal end of the structure for adhesion. Although no significant primary sequence similarity can be detected with proteins of known structure (no E value < 1 PHYRE hits (67)), both domains display structural similarity to two separate families of surface proteins from Gram positive bacteria (68).

The structure of the β -domain resembles the ligand-binding A-region from the Microbial Surface Components Recognizing Adhesive Matrix Molecules (MSCRAMM) family of bacterial adhesins (Supplementary Fig. S8A). Specifically, a high degree of similarity is observed with the fibrinogen-binding protein SdrG from *S. epidermidis* (pdb:1r17; Supplementary Fig. S8A) (55,69-70), the collagen binding ACE from *Enterococcus faecalis* (pdb:2z1p; Supplementary Fig. S8B) (71-72) and the clumping factor A from *S. aureus* (pdb:1n67; Supplementary Fig. S8C) (73-75); typically with a backbone RMSD of 3.5 Å over ~120 residues. The MSCRAMM ligand-binding region encompasses two similar β -domains, in which a ligand peptide docks into an inter-domain groove of the open structure and a C-terminal extension closes the complex resulting in a change in relative domain orientation (74). Although the α -domain is unrelated to the flanking β -rich domain from the MSCRAMMs, it displays a striking similarity with the imperfect helical repeats of EBH, the giant, extracellular matrix-binding protein from staphylococci (pdb:2dgi; Supplementary Fig. S8D) (76). The lack of electron density for the α -domain within the crystal structure of Fap1-NR, coupled with its well-defined structure in solution also implies that some flexibility exists at the interdomain boundary. It is tempting to speculate that the dual similarity with EBH and MSCRAMM surface proteins implies that host extracellular matrix proteins (ECM) are putative targets for Fap1 and supports the wider role for SRR fimbriae. The interaction between Fap1 and the salivary pellicle also suggests a role for calcium binding, however, no direct interaction was observable in our NMR assays (data not shown).

Fap1 exhibits an unusual pH-dependent conformational change that affects key residues located at the interdomain junction of the two subdomains of Fap1-NR, with concomitant effects on the relative arrangement of these domains that

allow Fap1 to adhere more tightly to SHA. The mean resting saliva pH observed in human oral cavities lies in the range 6.5 to 7.1. However, the buffering capacity of saliva is unable to cope with the rapid drop in pH induced by microbial acid production after the ingestion of fermentable carbohydrates. Plaque pH can reach values below 5.0 and remain low for some time before returning to neutrality. Some streptococci, particularly *S. mutans*, alter their physiology to survive in acidic environments. This is known as the acid tolerance response (ATR) and includes the production of stress-responsive proteins, increased glycolytic activity and the regulation of intracellular pH (77-78). *S. parasanguinis* and many other oral streptococci are primary colonisers of the oral cavity and will be frequently exposed to acidic stress; however, they are unable to thrive at low pH and in response shut down their metabolic functions (79). A plausible mechanism for survival would be for *S. parasanguinis* to modulate adhesion to outcompete acid-tolerant species, a mechanism that has been proposed for other species of bacteria (80-84). Enhanced Fap1-mediated adhesion at low pH would provide a more tenacious attachment to the salivary pellicle and increase the likelihood of *S. parasanguinis* survival during periods of acidic conditions. Moreover, its role as substrate for biofilm formation would also be enhanced thereby increasing bacterial cell density and providing respite.

Using a combination of low and high resolution methods we provide new insights into the architecture of Fap1 fimbriae and adhesion by a primary coloniser of the human oral cavity. Furthermore, our conclusions likely extend to other SRR fimbriae from pathogenic organisms and suggest new therapeutic strategies.

ACKNOWLEDGEMENTS

The authors would like to thank the Wellcome Trust (programme grant number 079819; equipment grant number 085464 to

SM) and the National Institutes of Health (grant R01DE017474 awarded to TR, and grants R01DE011000 and R01DE017954 to HW) for financial support. We would like to thank the beamline scientists at ID29 of the European Synchrotron Radiation Facility (ESRF) and X33 at the DORIS-III ring of

the Deutsches Elektronen-Synchrotron (DESY). The authors are also indebted to Christina Redfield at Oxford University for the provision of 950 MHz instrument time. The 950 MHz NMR facility was funded by the Wellcome Trust Joint Infrastructure Fund (JIF) and the E.P. Abraham Fund.

REFERENCES

1. Fux, C. A., Costerton, J. W., Stewart, P. S., and Stoodley, P. (2005) *Trends in Microbiology* **13**, 34-40
2. Mandlik, A., Swierczynski, A., Das, A., and Ton-That, H. (2008) *Trends in Microbiology* **16**, 33-40
3. Costerton, J. W., Stewart, P. S., and Greenberg, E. P. (1999) Bacterial Biofilms: A Common Cause of Persistent Infections. in *Science*
4. Nobbs, A. H., Lamont, R. J., and Jenkinson, H. F. (2009) *Microbiol. Mol. Biol. Rev.* **73**, 407-450
5. Kreth, J., Merritt, J., and Qi, F. (2009) *DNA and Cell Biology* **28**, 397-403
6. Paju, S., and Scannapieco, F. A. (2007) *Oral Diseases* **13**, 508-512
7. Scannapieco, F. A., Bush, R. B., and Paju, S. (2003) *Ann Periodontol* **8**, 38-53
8. Fujitani, S., Rowlinson, M. C., and George, W. L. (2008) *Clinical Infectious Diseases* **46**, 1064-1066
9. Giannitsioti, E., Chirouze, C., Bouvet, A., Beguinot, I., Delahaye, F., Mainardi, J. L., Celard, M., Mihaila-Amrouche, L., Moing, V. L., Hoen, B., and Grp, A. S. (2007) *Clinical Microbiology and Infection* **13**, 770-776
10. Westling, K., Julander, I., Ljungman, P., Jalal, S., Nord, C. E., and Wretling, B. (2006) *International Journal of Antimicrobial Agents* **28**, 292-296
11. Stephenson, A. E., Wu, H., Novak, J., Tomana, M., Mintz, K., and Fives-Taylor, P. (2002) *Molecular Microbiology* **43**, 147-157
12. Wu, H., and Fives-Taylor, P. M. (1999) *Molecular Microbiology* **34**, 1070-1081
13. Stephenson, A., and Fives-Taylor, P. (1998) *Journal of Dental Research* **77**, 133
14. Wu, H., Mintz, K. P., Ladha, M., and Fives-Taylor, P. M. (1998) *Molecular Microbiology* **28**, 487-500
15. Froeliger, E. H., and Fives-Taylor, P. (2001) *Infection and Immunity* **69**, 2512-2519
16. Rigel, N. W., and Braunstein, M. (2008) *Molecular Microbiology* **69**, 291-302
17. Xiong, Y. Q., Bensing, B. A., Bayer, A. S., Chambers, H. F., and Sullam, P. M. (2008) *Microbial Pathogenesis* **45**, 297-301
18. Siboo, I. R., Chambers, H. F., and Sullam, P. M. (2005) *Infect. Immun.* **73**, 2273-2280
19. van Sorge, N. M., Quach, D., Gurney, M. A., Sullam, P. M., Nizet, V., and Doran, K. S. (2009) *Journal of Infectious Diseases* **199**, 1479-1487
20. Shivshankar, P., Sanchez, C., Rose, L. F., and Orihuela, C. J. (2009) *Molecular Microbiology* **73**, 663-679
21. Mistou, M. Y., Dramsi, S., Brega, S., Poyart, C., and Trieu-Cuot, P. (2009) *Journal of Bacteriology* **191**, 4195-4206
22. Seifert, K. N., Adderson, E. E., Whiting, A. A., Bohnsack, J. F., Crowley, P. J., and Brady, L. J. (2006) *Microbiology-Sgm* **152**, 1029-1040
23. Sattler, M., Schleucher, J., and Griesinger, C. (1999) *Progress in NMR Spectroscopy*. **34**, 93-158

24. Ottiger, M., Delaglio, F., and Bax, A. (1998) *Journal of Magnetic Resonance* **131**, 373-378
25. Pervushin, K., Riek, R., Wider, G., and Wuthrich, K. (1997) *Proceedings of the National Academy of Sciences of the United States of America* **94**, 12366-12371
26. Delaglio, F., Grzesiek, S., Vuister, G. W., Zhu, G., Pfeifer, J., and Bax, A. (1995) *Journal of Biomolecular Nmr* **6**, 277-293
27. Johnson, B. A., and Blevins, R. A. (1994) *Journal of Biomolecular Nmr* **4**, 603-614
28. Bardiaux, B., Bernard, A., Rieping, W., Habeck, M., Malliavin, T. E., and Nilges, M. (2009) *Proteins-Structure Function and Bioinformatics* **75**, 569-585
29. Rieping, W., Habeck, M., Bardiaux, B., Bernard, A., Malliavin, T. E., and Nilges, M. (2007) *Bioinformatics* **23**, 381-382
30. Brunger, A. T., Adams, P. D., Clore, G. M., DeLano, W. L., Gros, P., Grosse-Kunstleve, R. W., Jiang, J. S., Kuszewski, J., Nilges, M., Pannu, N. S., Read, R. J., Rice, L. M., Simonson, T., and Warren, G. L. (1998) *Acta Crystallographica Section D-Biological Crystallography* **54**, 905-921
31. Cornilescu, G., Delaglio, F., and Bax, A. (1999) *Journal of Biomolecular Nmr* **13**, 289-302
32. Clore, G. M., Gronenborn, A. M., and Bax, A. (1998) *Journal of Magnetic Resonance* **133**, 216-221
33. Dosset, P., Hus, J. C., Marion, D., and Blackledge, M. (2001) *Journal of Biomolecular Nmr* **20**, 223-231
34. Nilges, M., Bernard, A., Bardiaux, B., Malliavin, T., Habeck, M., and Rieping, W. (2008) *Structure* **16**, 1305-1312
35. Linge, J. P., Habeck, M., Rieping, W., and Nilges, M. (2003) *Bioinformatics* **19**, 315-316
36. CCP4. (1994) *Acta Crystallographica* **D50**, 760-763
37. Schneider, T. R., and Sheldrick, G. M. (2002) *Acta Crystallographica Section D-Biological Crystallography* **58**, 1772-1779
38. Emsley, P., and Cowtan, K. (2004) *Acta Crystallographica Section D-Biological Crystallography* **60**, 2126-2132
39. Murshudov, G. N., Vagin, A. A., and Dodson, E. J. (1997) *Acta Crystallographica Section D-Biological Crystallography* **53**, 240-255
40. Konarev, P. V., Volkov, V. V., Sokolova, A. V., Koch, M. H. J., and Svergun, D. I. (2003) *Journal of Applied Crystallography* **36**, 1277-1282
41. Petoukhov, M. V., and Svergun, D. I. (2003) *Journal of Applied Crystallography* **36**, 540-544
42. Wriggers, W., and Chacon, P. (2001) *Journal of Applied Crystallography* **34**, 773-776
43. Miller, D. J., Jerga, A., Rock, C. O., and White, S. W. (2008) *Structure* **16**, 1036-1046
44. Fives-Taylor, P. M., and Thompson, D. W. (1985) *Infection and Immunity* **47**, 752-759
45. Ruiz, T., Mechin, I., Bar, J., Rypniewski, W., Kopperschlager, G., and Radermacher, M. (2003) *Journal of Structural Biology* **143**, 124-134
46. Frank, J., Radermacher, M., Penczek, P., Zhu, J., Li, Y. H., Ladjadj, M., and Leith, A. (1996) *Journal of Structural Biology* **116**, 190-199
47. Radermacher, M., Ruiz, T., Wiczorek, H., and Gruber, G. (2001) *Journal of Structural Biology* **135**, 26-37
48. Ludtke, S. J., Baldwin, P. R., and Chiu, W. (1999) *Journal of Structural Biology* **128**, 82-97
49. Zhou, M. X., and Wu, H. (2009) *Microbiology-Sgm* **155**, 317-327

50. Plummer, C., Wu, H., Kerrigan, S. W., Meade, G., Cox, D., and Douglas, C. W. I. (2005) *British Journal of Haematology* **129**, 101-109
51. Takamatsu, D., Bensing, B. A., Cheng, H., Jarvis, G. A., Siboo, I. R., Lopez, J. A., Griffiss, J. M., and Sullam, P. M. (2005) *Molecular Microbiology* **58**, 380-392
52. Takamatsu, D., Bensing, B. A., Prakobphol, A., Fisher, S. J., and Sullam, P. M. (2006) *Infection and Immunity* **74**, 1933-1940
53. Wu, H., Bu, S., Newell, P., Chen, Q., and Fives-Taylor, P. (2007) *Journal of Bacteriology* **189**, 1390-1398
54. Fronzes, R., Remaut, H., and Waksman, G. (2008) *EMBO J* **27**, 2271-2280
55. Bowden, M. G., Heuck, A. P., Ponnuraj, K., Kolosova, E., Choe, D., Gurusiddappa, S., Narayana, S. V. L., Johnson, A. E., and Hook, M. (2008) *Journal of Biological Chemistry* **283**, 638-647
56. Ton-That, H., and Schneewind, O. (2004) *Trends in Microbiology* **12**, 228-234
57. Samen, U., Reinscheid, D. J., Reinscheid, D. J., and Borges, F. (2007) *Infection and Immunity* **75**, 5405-5414
58. Wu, H., Zeng, M., and Fives-Taylor, P. (2007) *Infection and Immunity* **75**, 2181-2188
59. Kajava, A. V. (2001) *Journal of Structural Biology* **134**, 132-144
60. Shoulders, M. D., and Raines, R. T. (2009) *Annual Review of Biochemistry* **78**, 929-958
61. Asakura, T., Ohgo, K., Komatsu, K., Kanenari, M., and Okuyama, K. (2005) *Macromolecules* **38**, 7397-7403
62. Sangappa, Mahesh, S. S., and Somashekar, R. (2005) *Journal of Biosciences* **30**, 259-268
63. Ghasparian, A., Moehle, K., Linden, A., and Robinson, J. A. (2006) *Chemical Communications*, 174-176
64. Plassmeyer, M. L., Reiter, K., Shimp, R. L., Kotova, S., Smith, P. D., Hurt, D. E., House, B., Zou, X. Y., Zhang, Y. L., Hickman, M., Uchime, O., Herrera, R., Nguyen, V., Glen, J., Lebowitz, J., Jin, A. J., Miller, L. H., MacDonald, N. J., Wu, Y. M., and Narum, D. L. (2009) *Journal of Biological Chemistry* **284**, 26951-26963
65. Handley, P. S., Correia, F. F., Russell, K., Rosan, B., and DiRienzo, J. M. (2005) *Oral Microbiology and Immunology* **20**, 131-140
66. Hilleringmann, M., Ringler, P., Muller, S. A., De Angelis, G., Rappuoli, R., Ferlenghi, I., and Engel, A. (2009) *EMBO J* **28**, 3921-3930
67. Kelley, L. A., and Sternberg, M. J. E. (2009) *Nat. Protocols* **4**, 363-371
68. Holm, L., Kaariainen, S., Rosenstrom, P., and Schenkel, A. (2008) *Bioinformatics* **24**, 2780-2781
69. Ponnuraj, K., Bowden, M. G., Davis, S., Gurusiddappa, S., Moore, D., Choe, D., Xu, Y., Hook, M., and Narayana, S. V. L. (2003) *Cell* **115**, 217-228
70. Hartford, O., O'Brien, L., Schofield, K., Wells, J., and Foster, T. J. (2001) *Microbiology-Sgm* **147**, 2545-2552
71. Sillanpaa, J., Nallapareddy, S. R., Houston, J., Ganesh, V. K., Bourgoigne, A., Singh, K. V., Murray, B. E., and Hook, M. (2009) *Microbiology-Sgm* **155**, 2390-2400
72. Liu, Q., Ponnuraj, K., Xu, Y., Ganesh, V. K., Sillanpaa, J., Murray, B. E., Narayana, S. V. L., and Hook, M. (2007) *Journal of Biological Chemistry* **282**, 19629-19637
73. Deivanayagam, C. C. S., Wann, E. R., Chen, W., Carson, M., Rajashankar, K. R., Hook, M., and Narayana, S. V. L. (2002) *EMBO J* **21**, 6660-6672
74. Ganesh, V. K., Rivera, J. J., Smeds, E., Ko, Y. P., Bowden, M. G., Wann, E. R., Gurusiddappa, S., Fitzgerald, J. R., and Hook, M. (2008) *Plos Pathogens* **4**
75. Keane, F. M., Loughman, A., Valtulina, V., Brennan, M., Speziale, P., and Foster, T. J. (2007) *Molecular Microbiology* **63**, 711-723

76. Tanaka, Y., Sakamoto, S., Kuroda, M., Goda, S., Gao, Y. G., Tsumoto, K., Hiragi, Y., Yao, M., Watanabe, N., Ohta, T., and Tanaka, I. (2008) *Structure* **16**, 488-496
77. Takahashi, N., and Yamada, T. (1999) *Oral Microbiology and Immunology* **14**, 43-48
78. Welin-Neilands, J., and Svensater, G. (2007) *Applied and Environmental Microbiology* **73**, 5633-5638
79. Svensater, G., Larsson, U. B., Greif, E. C. G., Cvitkovitch, D. G., and Hamilton, I. R. (1997) *Oral Microbiology and Immunology* **12**, 266-273
80. Brooks, D. E., and Trust, T. J. (1983) *Journal of General Microbiology* **129**, 3661-3669
81. Guglielmetti, S., Tamagnini, I., Minuzzo, M., Arioli, S., Parini, C., Comelli, E., and Mora, D. (2009) *Current Microbiology* **59**, 167-172
82. Ito, H. O., Soutome, S., and Inoue, M. (2003) *Journal of Microbiological Methods* **55**, 29-34
83. Kim, S. B., Park, S. J., Lee, C. G., Choi, N. C., and Kim, D. J. (2008) *Colloids and Surfaces B-Biointerfaces* **63**, 236-242
84. Takai, S., Yanagawa, R., and Kitamura, Y. (1980) *Infection and Immunity* **28**, 669-674
85. Davis, I. W., Leaver-Fay, A., Chen, V. B., Block, J. N., Kapral, G. J., Wang, X., Murray, L. W., Arendall, W. B., Snoeyink, J., Richardson, J. S., and Richardson, D. C. (2007) *Nucleic Acids Res* **35**, 375-383
86. Laskowski, R. A., Macarthur, M. W., Moss, D. S., and Thornton, J. M. (1993) *Journal of Applied Crystallography* **26**, 283-291
87. Vriend, G. (1990) *Journal of Molecular Graphics* **8**, 52-&

Figure Captions

Fig. 1: Domain organisation of *S. parasanguinis* Fap1 and adhesion to SHA

- Schematic representation of the domain structure of Fap1. The amino acid positions at which the domains begin and end are indicated. Mature Fap1 is numbered 1 to 2502.
- Fap1-NR, Fap1-NR $_{\alpha}$ and Fap1-NR $_{\beta}$ block bacterial adhesion in a dose dependent manner. 0, 10 and 100 μ g of recombinant Fap1 proteins were preincubated with SHA before adding 3 H thymidine labelled wild-type *S. parasanguinis*. Wild-type binding is normalised to 100% and the *fap1* deletion mutant was used as a negative control.

Fig. 2: Three-dimensional structures of the two sub-domains Fap1-NR $_{\alpha}$ and Fap1-NR $_{\beta}$ from the major non-repeat region from *S. parasanguinis* Fap1 fimbriae.

- Ribbon representation of the X-ray structure of Fap1-NR $_{\beta}$. The β -strands are colored in yellow and orange, short helices in red. L1 to L9 refer to loops 1 to 9 in the structure.
- Topology diagram of the X-ray structure of Fap1-NR $_{\beta}$ with the same colored code as in (a).
- Superimposition of the ten best NMR structures of Fap1-NR $_{\alpha}$ with the three helices α 1, α 2 and α 3 shown in blue.
- Ribbon representation of the NMR structure of Fap1-NR $_{\alpha}$ in two different orientations with the three helices α 1, α 2 and α 3 in blue. Leucine, alanine and isoleucine side-chains involved in inter-helix interactions are colored in dark blue, cyan and magenta respectively.

Fig. 3: pH-dependent structural change in Fap1-NR $_{\alpha}$

- S. parasanguinis* adhesion to SHA is pH dependent. Adhesion of 3 H labelled wild-type bacteria to SHA was carried out at pH 5.0, 6.0, 7.0, 8.0 and 9.0.
- Superimposition of regions from the 15 N- 1 H HSQC spectra of Fap1-NR $_{\alpha}$ measured at 500 MHz at pH 8.0 (blue), pH 6.2 (black), pH 5.7 (green) and pH 5.2 (red). Full TROSY-HSQC spectra of Fap1-NR are shown in Supplementary fig. S7.
- Weighted differences in the observed 1 H and 15 N chemical shifts of Fap1-NR $_{\alpha}$ between pH 8.0 and pH 5.2, where $\Sigma\delta\text{ppm} = (4 \times \delta^1\text{H}) + \delta^{15}\text{N}$. Residues significantly affected by pH ($\Sigma\delta\text{ppm} > 0.95$) are highlighted in red, whilst those affected to a lesser extent ($0.95 < \Sigma\delta\text{ppm} > 0.8$) are highlighted in yellow. The secondary structure of the helical bundle is shown on the top. More details are also given in Supplementary Figs. S7 & S8.
- Localisation of the chemical shift changes between pH 8 and 5.2 on the NMR structure of Fap1-NR $_{\alpha}$ at pH 8. The three helices and the surface not affected by pH are in blue, whilst residues displaying chemical shift changes due to pH are colored in red (large) and yellow (small). The orientation is the same as Fig 2C. The chemical shift changes are localised towards the C-terminal pole.

Fig. 4: Overall structure of Fap1-NR and mutagenesis

- SAXS scattering profile of Fap1-NR at pH 5 (red) and pH 8 (blue).
- SAXS derived electron density for Fap1-NR at pH 8 with the crystal structure of Fap1-NR $_{\beta}$ and the solution structure of Fap1-NR $_{\alpha}$ rigid body fitted into the envelope. The 27 residue linker is shown as a blue dashed line and the N- and C-termini of Fap1-NR are annotated.
- Effects of pH change on the electron density of Fap1-NR. SAXS derived electron density at pH 8 is blue and at pH 5 is red.
- Potential receptor binding surface of Fap1. Two exposed hydrophobic regions were mutated Fap1-NR. Residues including I134, E138, D142, L163 and V164 in Fap1-NR $_{\alpha}$ together with L385, I291, L292, L300, N403, Q405 and I411 in Fap1-NR $_{\beta}$ were mutated to alanine. Mutants affecting adhesion of Fap1-NR are shown as green spheres and line the concave face of the SAXS envelope. The position of the negative control E204A is shown as yellow spheres and is on the non-concave face. Residues in Fap1-NR $_{\alpha}$ affected by changes in pH are colored red and congregate at the interdomain boundary.
- Effect of site-directed mutagenesis of amino acid residues located at the putative binding interfaces in Fap1-NR on bacterial adhesion to SHA. Adhesion of *S. parasanguinis* FW213 (1), *fap1* mutant (2) and site-directed *fap1* mutants: I134A (3), E138A (4), I134AE138A (5), D142A (6), L163A(7), V164A(8) and E204A (9) in the α -domain; and L385A(10), I411A (11), L300A (12), I291AL292A(13), N403A(14), Q405A(15) and N403AQ405A (16) in the β -domain.

Fig. 5: Electron microscopy of Fap1 fimbriae

- Micrographs of long fimbriae from wild type *S. parasanguinis* stained with UA (left), PTA (centre) and MAT (right). Scale bar = 100 nm; Black arrows indicate fimbriae; White arrows indicate tip aggregates; Open white arrows indicate fimbrial bundles.
- Averaging of narrow fimbrial sections; micrograph of *S. parasanguinis* stained with PTA (left), three representative fimbrial sections (centre) and average of all fimbrial regions (right). Scale bar = 10 nm; Fimbriae diameter 5.5 nm.
- Average power spectra from fimbrial regions stained with UA (left), PTA (middle) and MAT (right) lines show the principal 1/6.5 nm layer line and a weaker one at 1/33 nm, present in all staining conditions.

Fig. 6: Model for the super-coiled strand of Fap1 fimbriae.

The protomer is colored as in Fig. 1a with the cell wall anchor colored cyan, the major and minor SRR regions colored dark (protein) and light (glycan) orange, whilst the major and minor NR regions are colored green. The model on the left represents a super-coiled Fap1 monomer with repeating units of 6.5 nm along the fibre axis of the SRR region and protomer length of approximately 250-300 nm. Extra subunits may be incorporated within a coiled-coil to produce higher oligomeric states and the model on the right represents multiple

polymerized subunits with just two displayed here. The Fap1 model was created from a left-handed helix in which single atoms (representing individual amino acids) were arranged on a helical axis, with additional atoms (representing glycan residues) associated with alternate amino acid residues. This helix was in turn rotated about a central super-helical fibre axis. The SAXS envelope was scaled to the SRR model and placed at the C-termini, followed by a short stretch of the helical SRR model representing the minor SRR. An alignment of SRR sequences (middle) from *S. parasanguinis* Fap1, *S. aureus* SrpA, *S. gordonii* M99 GspB and *L. johnsonii* NCC533 LJ1711 is shown. The consensus SRR dipeptide sequence (SRRc) is SX, where X can be any amino acid.

Table 1: Crystal data collection and refinement statistics for Fap1-NR β .

Crystal parameters	
Space group	P 3 ₂ 2 1
Cell dimensions	a=b=108.67 Å c=126.25 Å
Data collection	
Beamline	ESRF ID29
Wavelength (Å)	0.97910
Resolution (Å)	2.90 (2.90-3.06)
Unique observations	19567 (2832)
R _{meas}	0.132 (0.47)
$\langle I \rangle / \sigma I$	15.2 (4.16)
Completeness (%)	99.84 (100.0)
Redundancy	7.88 (7.53)
Refinement	
R _{work} / R _{free} (%)	21.10 / 25.05
Number of protein residues	400
rmsd stereochemistry	
Bond lengths (Å)	0.02
Bond angles (°)	1.8
Ramachandran analysis (%)	
Residues in outlier regions	2 (Ser 246 A,B chain)
Residues in favoured regions	377 (95.2%)
Residues in allowed regions	394 (99.5%)

Numbers in parentheses refer to the outermost resolution shell.

$R_{\text{meas}} = \frac{\sum(h)(\sqrt{(n_h / (n_h - 1))} \sum(l) |I_{hl} - \langle I_h \rangle|}{\sum(h) \sum(l) \langle I_h \rangle}$ where I is the integrated intensity of a given reflection, $\langle I \rangle$ is the mean intensity of multiple corresponding symmetry-related reflections and n_h is the number of observations of reflection h .

$R_{\text{work}} = \frac{\sum ||F_o| - |F_c||}{\sum F_o}$ where F_o and F_c are the observed and calculated structure factors respectively.

$R_{\text{free}} = R_{\text{work}}$ calculated using ~5% random data excluded from the refinement.

rmsd stereochemistry is the deviation from ideal values.

Ramachandran analysis was carried out using *Molprobit* (85)

Table 2. NMR structural constraints and structure statistics for Fap1-NR_a.

Summary of structural constraints and structure statistics (PDB code 2kub)	
Number of restraints	
Distance restraints	
Intra-residue ($ i-j = 0$)	451
Sequential ($ i-j = 1$)	211
Medium-range ($2 \leq i-j < 5$)	256
Long-range ($ i-j \geq 5$)	103
Ambiguous	565
<i>Total</i>	1586
Dihedral angle restraints (φ/ψ)	138 (69/69)
Hydrogen bonds restraints	49
RDC restraints (D_{NH}/D_{CaHa})	38/54
Restraints statistics^a	
RMS of distance violations	
NOE restraints	$0.11 \pm 0.01 \text{ \AA}$
H-bonds restraints	$0.06 \pm 0.01 \text{ \AA}$
RMS of dihedral violations	$0.25 \pm 0.07^\circ$
RDC Q-factors	
D_{NH}	0.19 ± 0.04
D_{CaHa}	$0.31 \pm 0.01 \text{ Hz}$
RMS from idealized covalent geometry	
bonds	$0.0029 \pm 0.00008 \text{ \AA}$
angles	$0.49 \pm 0.009^\circ$
impropers	$1.45 \pm 0.06^\circ$
Structural quality^a	
<i>Ramachandran statistics^b</i>	
Most favoured regions	$99.2 \pm 0.9 \%$
Allowed regions	$0.8 \pm 0.9 \%$
Generously allowed regions	$0 \pm 0 \%$
Disallowed regions	$0 \pm 0 \%$
<i>WHAT-IF Z-score^c</i>	
Backbone conformation	1.90 ± 0.18
2 nd generation packing quality	4.32 ± 0.37
Ramachandran plot appearance	-0.82 ± 0.39
χ_1/χ_2 rotamer normality	-2.22 ± 0.17
Coordinates precision^d	
All backbone atoms	$0.39 \pm 0.06 \text{ \AA}$
All heavy atoms	$0.81 \pm 0.07 \text{ \AA}$

^a Average values and standard deviations over the 10 lowest-energy conformers

^b Percentage of residues in the Ramachandran plot regions determined by PROCHECK (86)

^c Z-scores values reported by WHAT-IF (87).

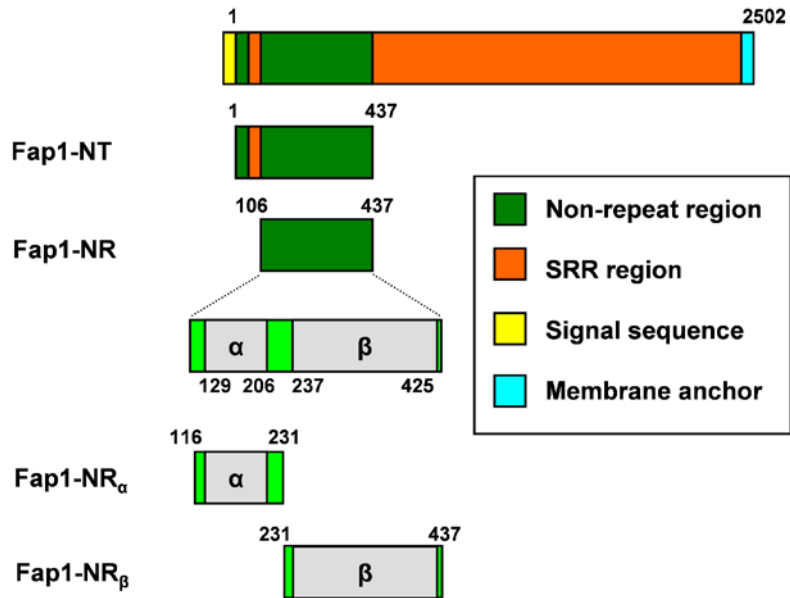
^d Average root mean square deviation (RMSD) over the 10 lowest-energy conformers' atomic coordinates with respect to the average structure.

Table3: SAXS data collection, processing and modelling statistics

<i>P(r)</i> function calculation	pH 5	pH 8
<i>q</i> -range (Å ⁻¹)	0.018-0.464	0.021-0.464
<i>R_g</i> (Å)	35.0 ± 0.2	36.2 ± 0.1
<i>I</i> (0)	88.5 ± 0.3	108.4 ± 0.3
<i>D_{max}</i> (Å)	127	128
Estimated molecular mass ^a	31 kDa	38 kDa
Mass calculated from sequence	37 kDa	37 kDa
<i>Ab initio</i> GASBOR modelling		
Ensemble average χ^2 to raw data	1.98 ± 0.07	2.15 ± 0.07
NSD ^b	1.11 ± 0.04	1.47 ± 0.07
<i>a.</i> By normalisation against data for BSA, calculated using the formula [<i>I</i> (0) _{FAP} ÷ <i>I</i> (0) _{BSA} *66 kDa] where <i>I</i> (0) _{BSA} was 188.3.		
<i>b.</i> For the definition of normalised spatial discrepancy (NSD), see Kozin & Svergun, 2001)		

Fig. 1

a)



b)

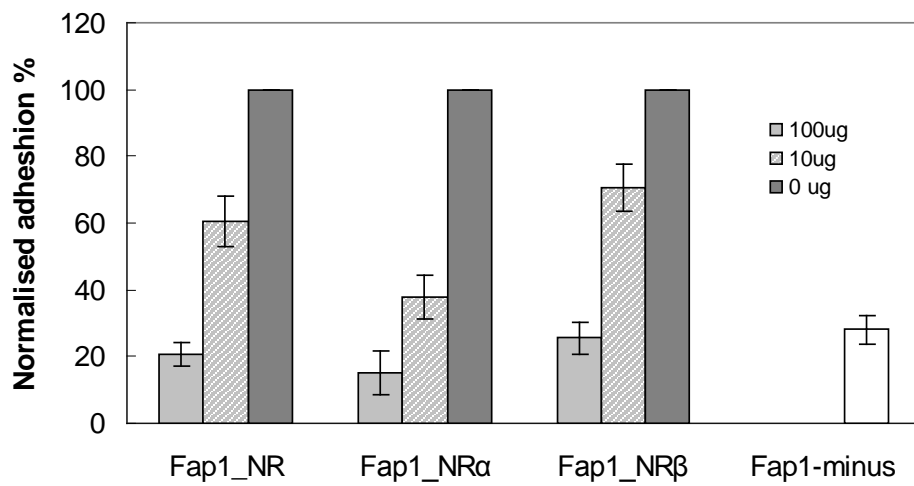


Fig. 2

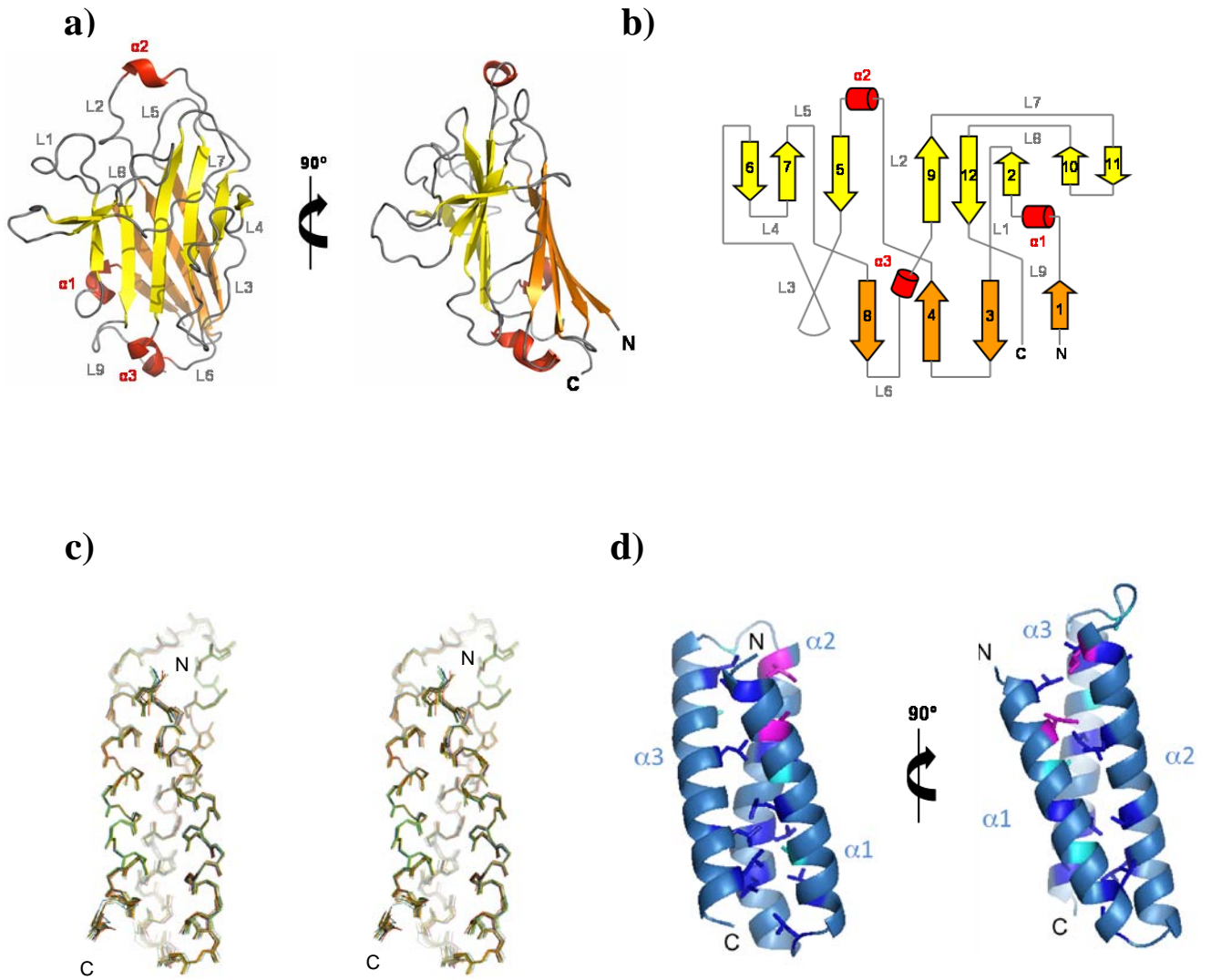
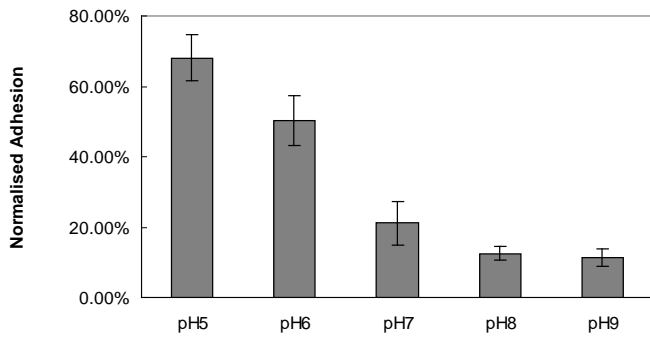
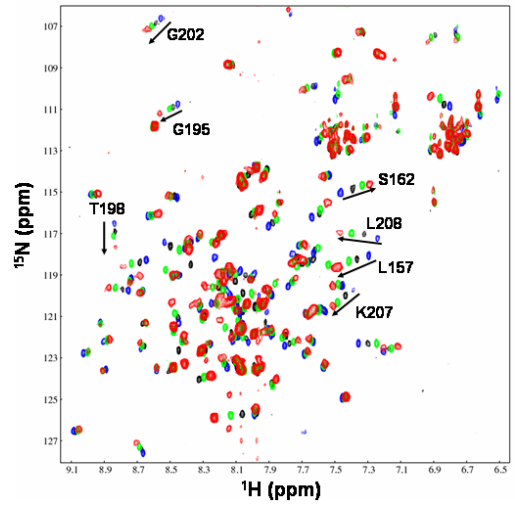


Fig. 3

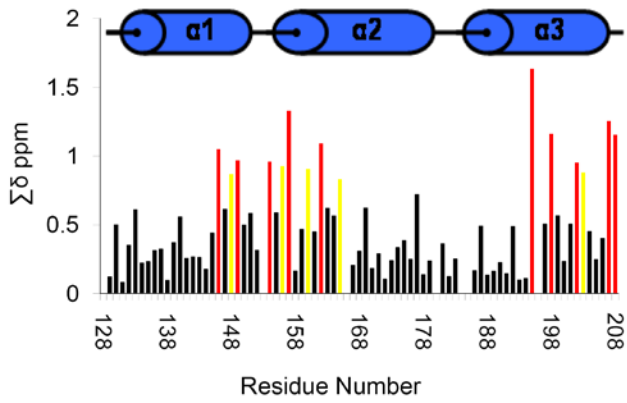
a)



b)



c)



d)

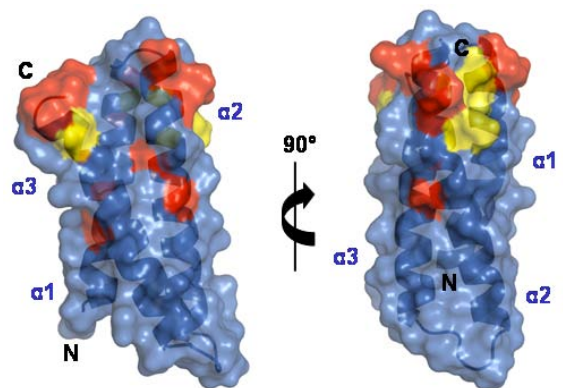


Fig. 4

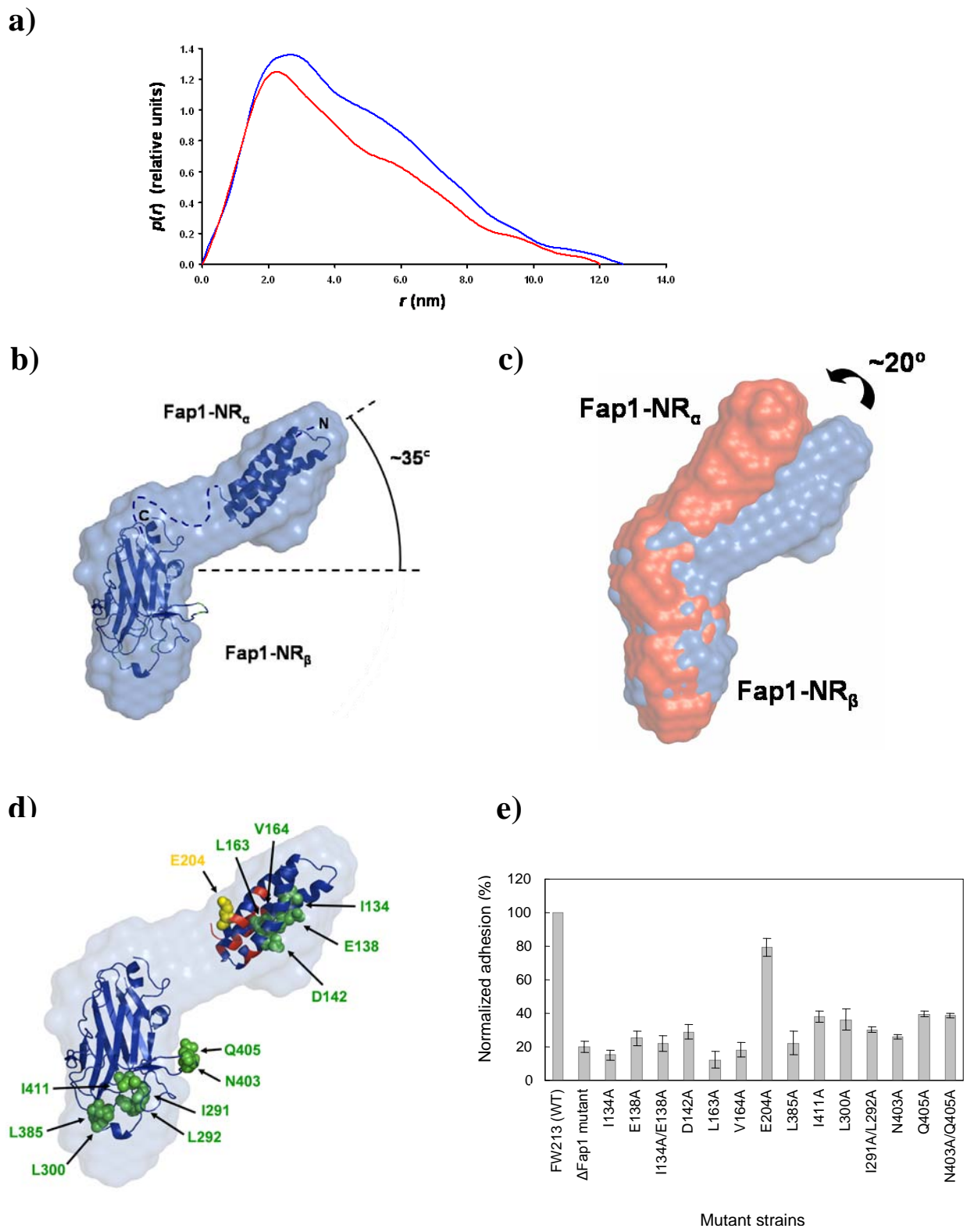
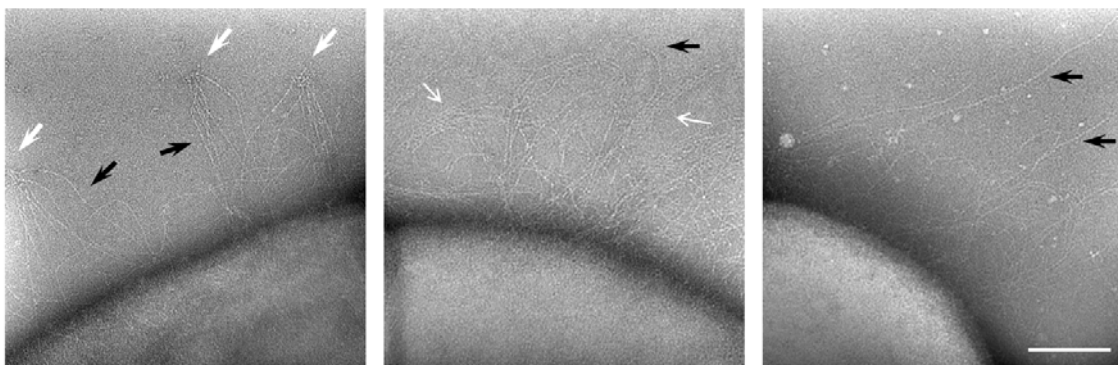
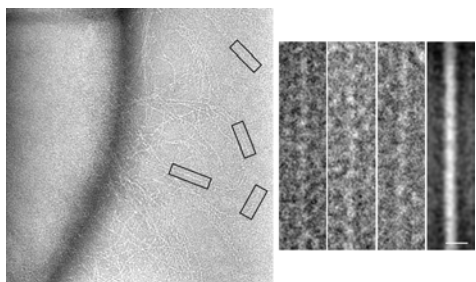


Fig. 5

a)



b)



c)

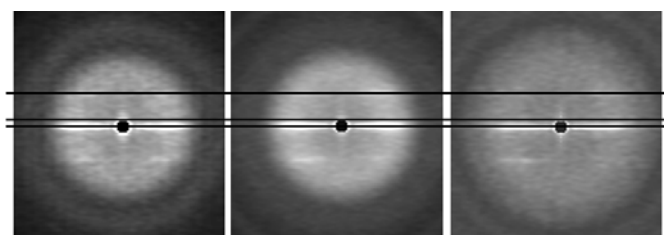
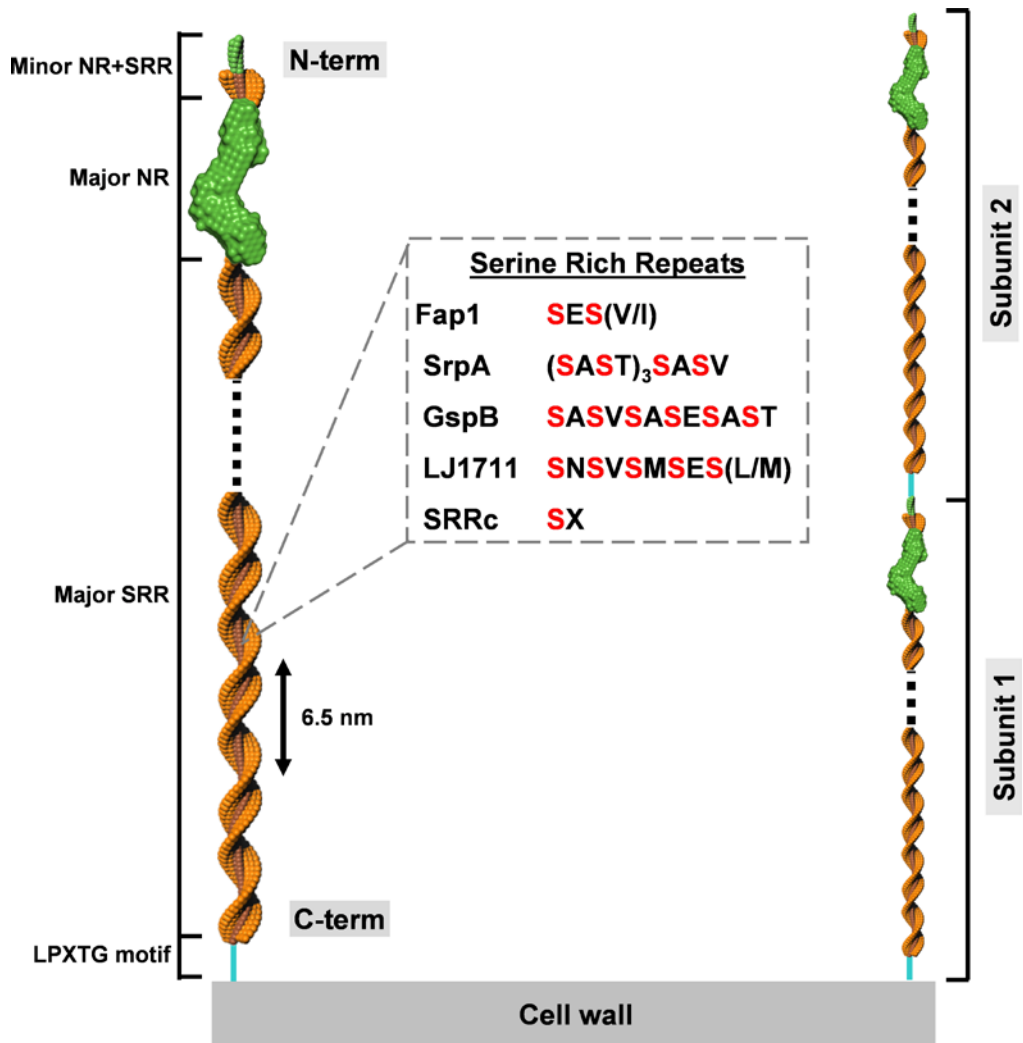


Fig. 6



Supplementary Data

STRUCTURAL INSIGHTS INTO SERINE-RICH FIMBRIAE FROM GRAM-POSITIVE BACTERIA

Stéphanie Ramboarina^{1§*}, James A. Garnett^{1*}, Meixian Zhou², Yuebin Li², Zhixiang Peng², Jonathan D. Taylor¹, Wei-chao Lee¹, Andrew Bodey¹, James W. Murray¹, Yilmaz Alguel¹, Julien Bergeron^{1,3}, Benjamin Bardiaux⁴, Elizabeth Sawyer¹, Rivka Isaacson¹, Camille Tagliaferri¹, Ernesto Cota¹, Michael Nilges⁵, Peter Simpson¹, and Teresa Ruiz⁶, Hui Wu^{2#} and Stephen Matthews^{1#}

¹*Department of Biological Sciences, Centre for Structural Biology, Imperial College London, South Kensington, London SW7 2AZ, UK.2*

²*Department of Paediatric Dentistry, University of Alabama at Birmingham, SDB 802, 1919 7th Avenue South, Birmingham, AL 35294-0007, USA*

³*Department of Infectious Diseases, King's College London School of Medicine, London, SE1 9RT, United Kingdom*

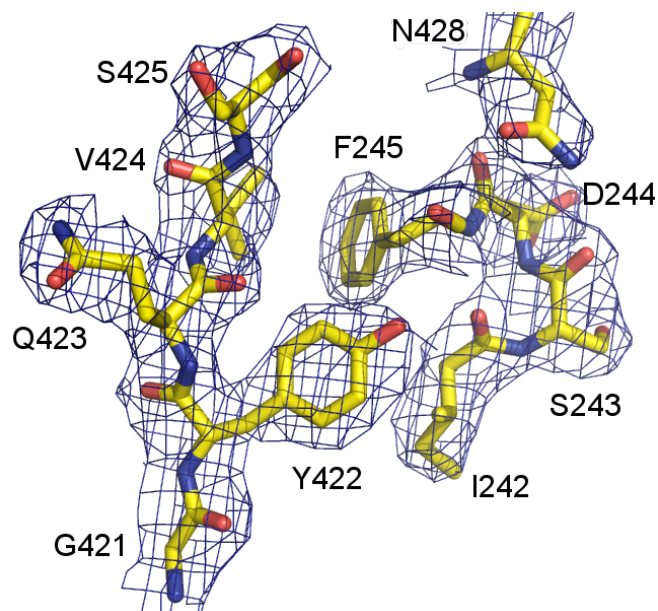
⁴*Structural Biology Unit, Leibniz Institute for Molecular Pharmacology, FMP Robert-Rossle –Str. 10. 13125 Berlin, Germany.*

⁵*Institut Pasteur Unité de Bioinformatique Structurale, 25-28 rue du Dr Roux, F-75724 Paris CEDEX 15, France*

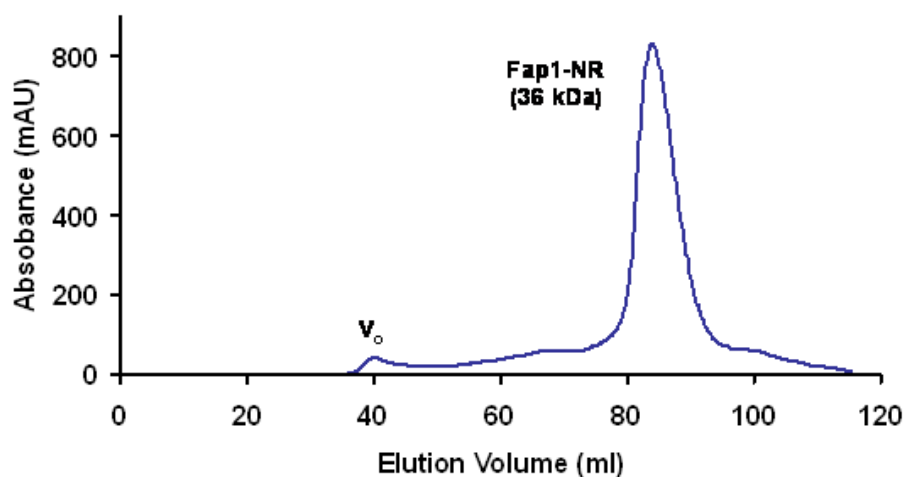
⁶*Molecular Physiology and Biophysics, University of Vermont, Burlington, VT 05405, USA*

[§] *Present address: Department of Molecular and Cellular Interactions, VIB Structural Biology Brussels, Vrije Universiteit Brussel, Pleinlaan 2, B-1050 Brussels, Belgium.*

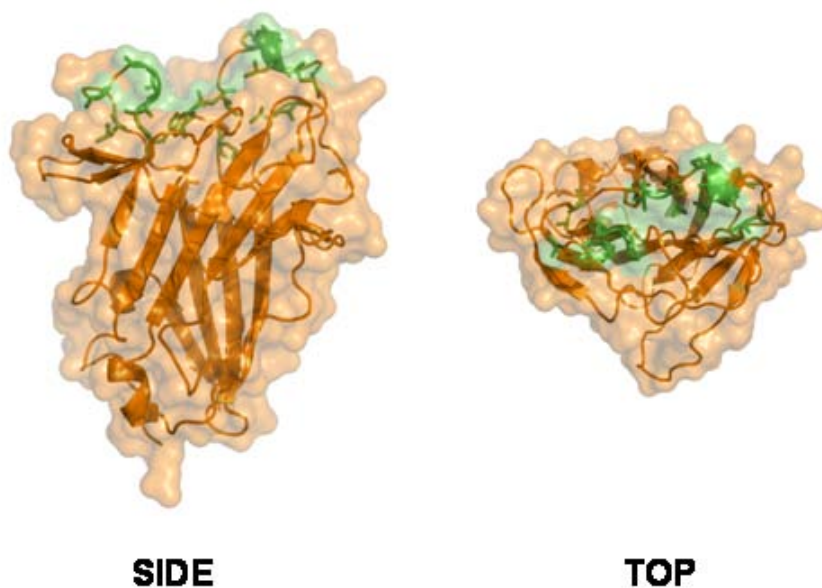
*These authors contributed equally; #Corresponding authors - SM (s.j.matthews@imperial.ac.uk) and HW(hwu@uab.edu)



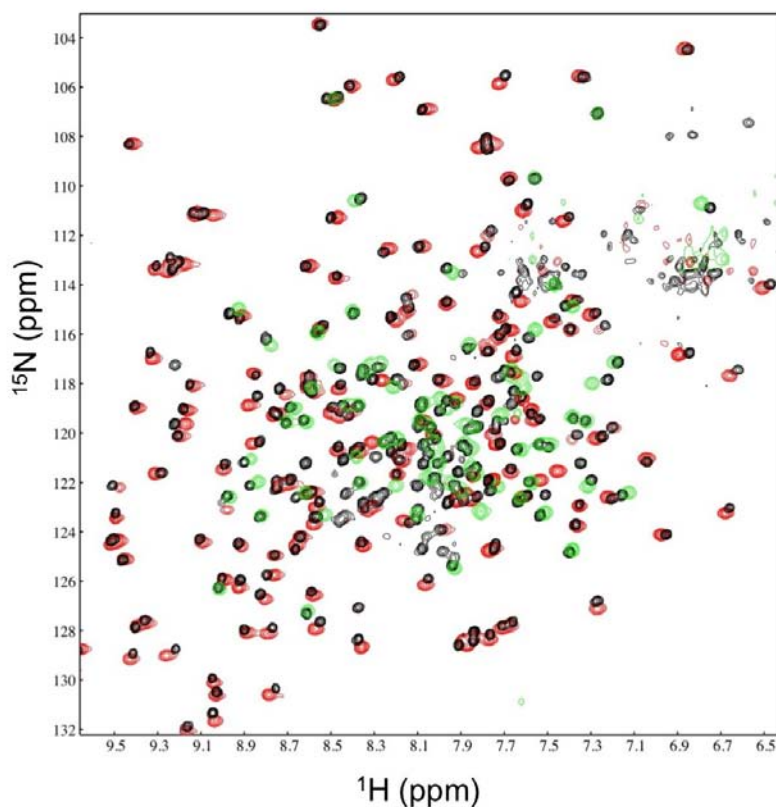
Supplementary Figure S1: An example of the electron density quality of the Fap1-NR β structure. Residues 242-245, 421-425 and 428 of chain A are shown as sticks with sigma A weighted maps contoured at 1 r.m.s electron density.



Supplementary Figure S2: Gel filtration profile of Fap1-NR performed on a Superdex-75 XK 16/60 column (GE healthcare). The void volume (V_o) and Fap1-NR elution volume are labelled. Predicted solution mass of Fap1-NR determined by SAXS experiments.

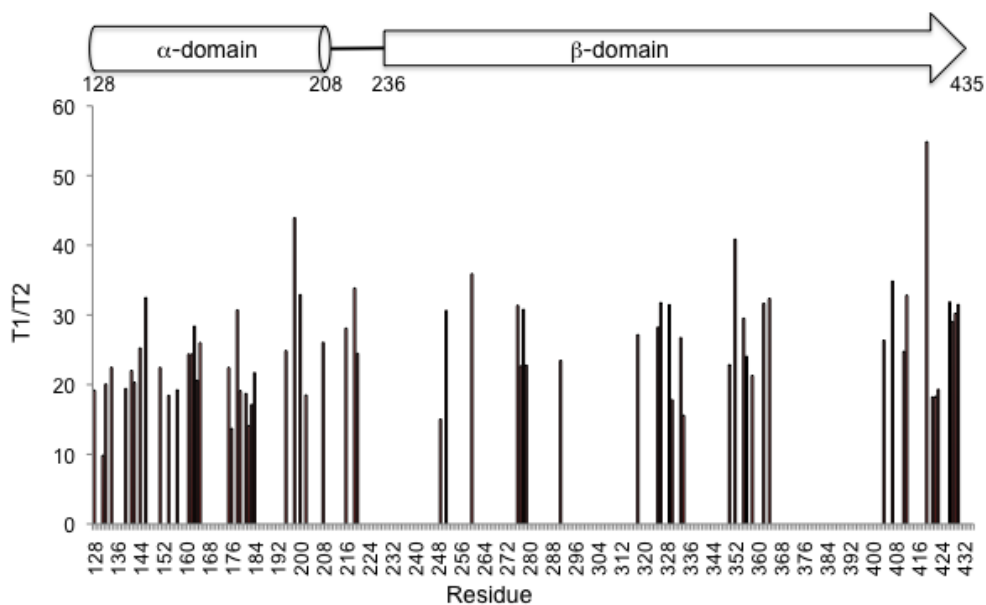
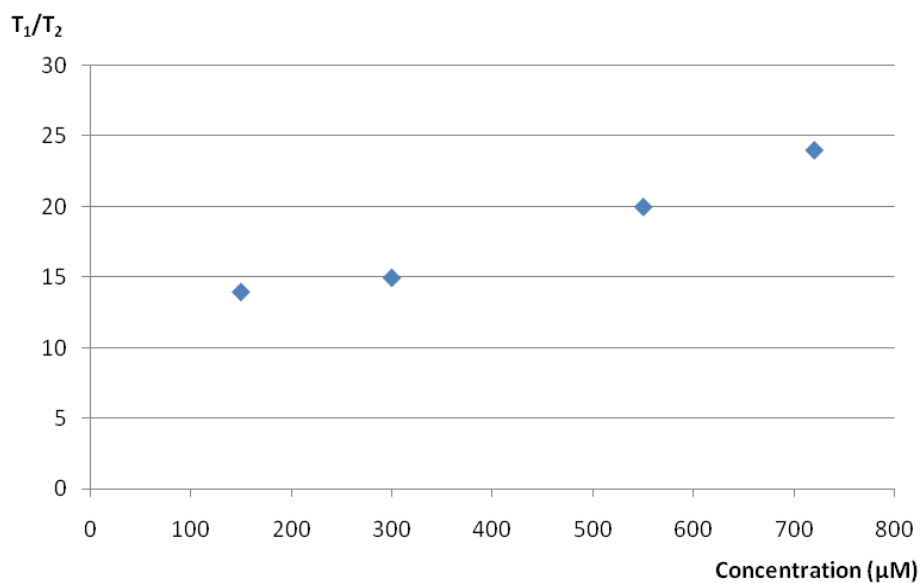


Supplementary Figure S3: Exposed hydrophobic region of Fap1-NR β loops L1-L2-L5. Fap1-NR β is coloured orange whilst hydrophobic residues clustered on the top side of the domain, within loops L1-L2-L5, are shown as green sticks.

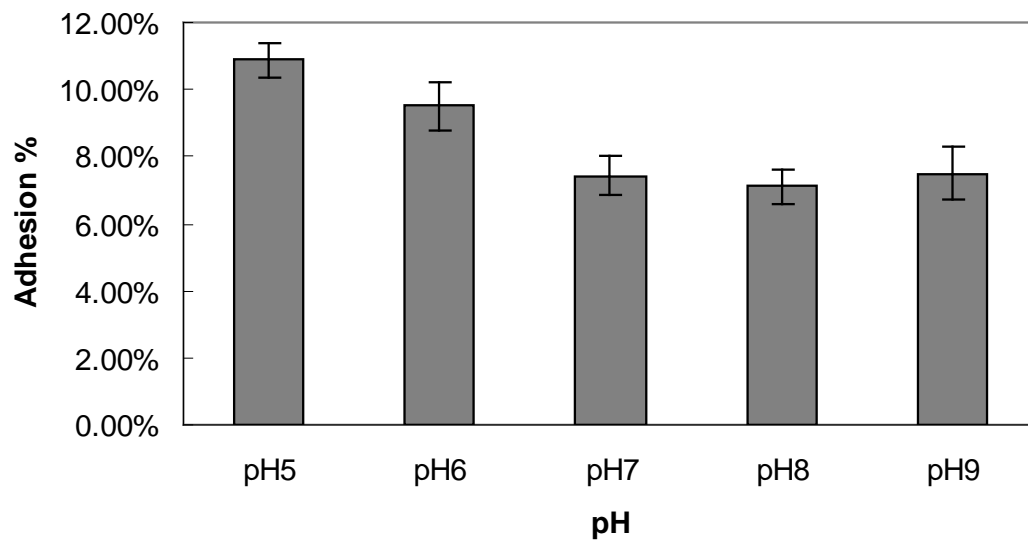


Supplementary Figure S4:

Superimposition of the 800MHz ^{15}N - ^1H TROSY-HSQC spectra of Fap1 fragments. Fap1-NR shown in black with both 800MHz ^1H - ^{15}N HSQC spectra of Fap1-NR α and Fap1-NR β in green and in red respectively at pH 8 and 303K.

a**b**

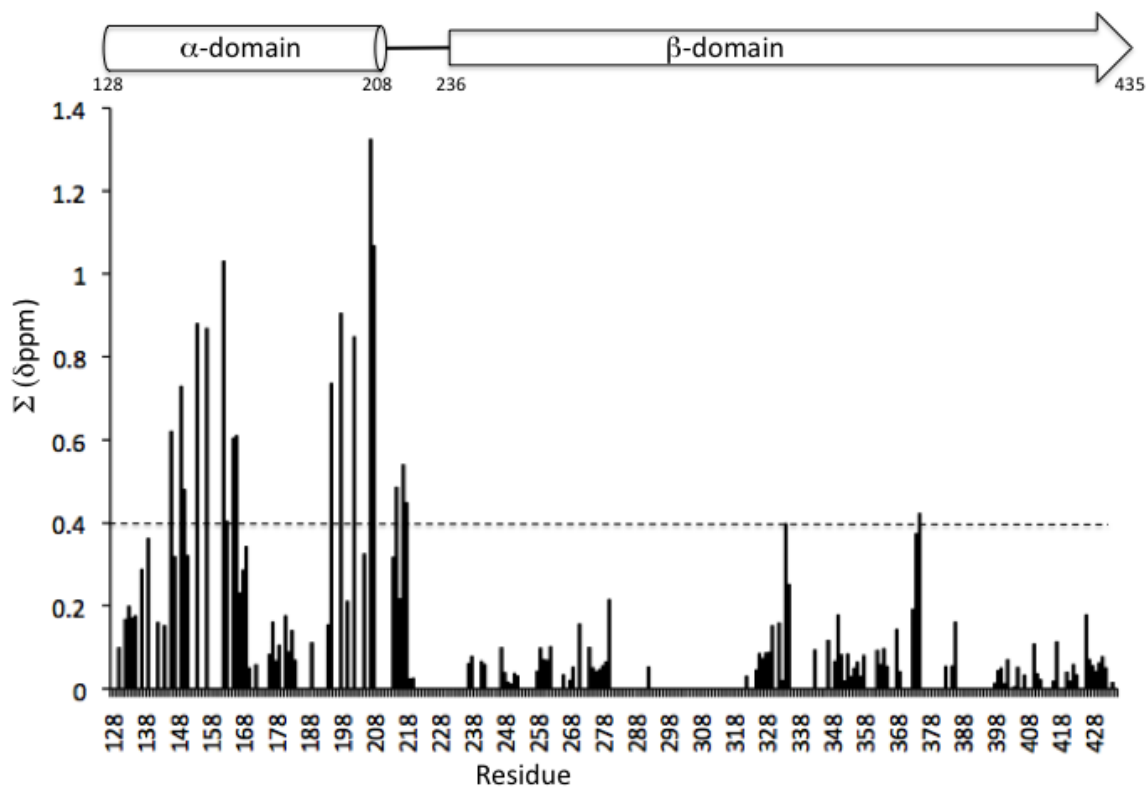
Supplementary Figure S5: (a) ^1H - ^{15}N T_1/T_2 measurements recorded for Fap1-NR. Differences in average T_1/T_2 ratios for α and β domains indicate some interdomain flexibility (b) ^1H - ^{15}N T_1/T_2 measurements recorded from Fap1-NR $_{\alpha}$ at 303K over a range of protein concentrations measured on a 500 MHz NMR spectrometer. Above ~ 300 μM Fap1-NR $_{\alpha}$ begins to self-associate into high molecular weight species.



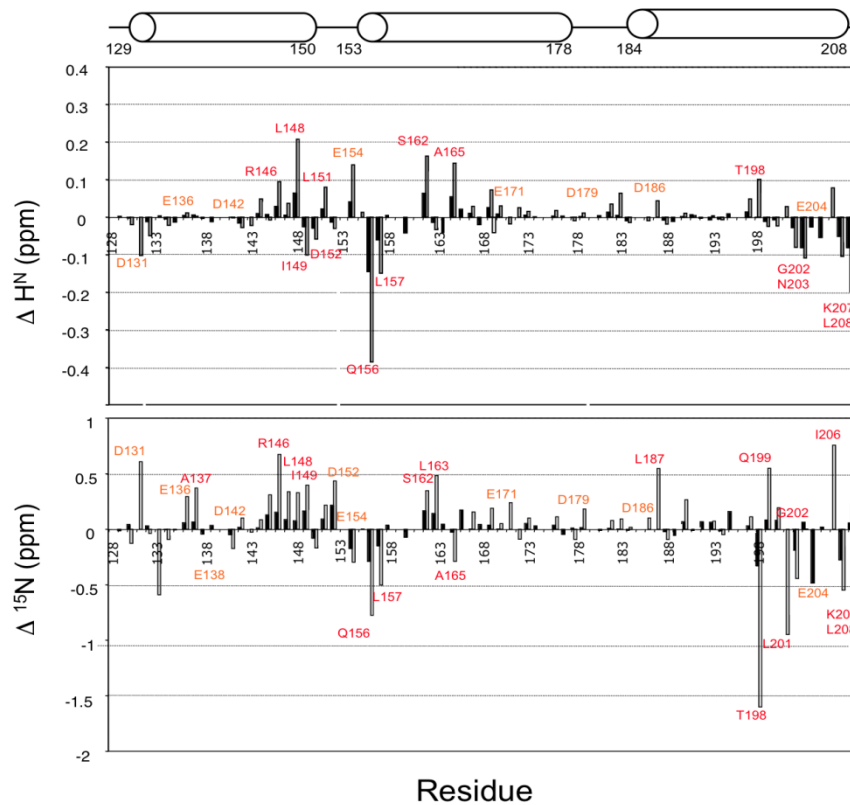
Supplementary Figure S6:

Adhesion of a *fap1* mutant of *S. parasanguinis* to SHA Adhesion of ³H labeled *fap1* mutant to SHA was carried out at pH 5.0, 6.0, 7.0, 8.0 and 9.0 as described in materials and methods.

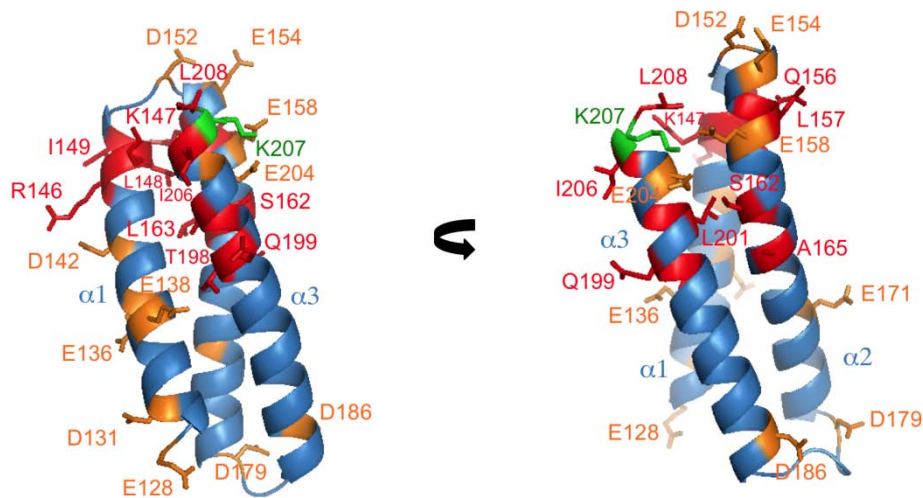
The *fap1* mutant exhibits only background level of adhesion at different conditions.



Supplementary Figure S7: pH-dependence of the NMR structure of Fap1-NR of *S. parasanguis* Fap1 fimbriae. Weighted differences in the observed ^1H and ^{15}N chemical shifts of Fap1-NR between pH 8.0 and pH 5.2, where $\Sigma\delta\text{ppm} = (4 \times \delta^1\text{H}) + \delta^{15}\text{N}$. The location of the individual domains is shown above. Gaps represent missing assignments for or severe overlap for some β -domain peaks.

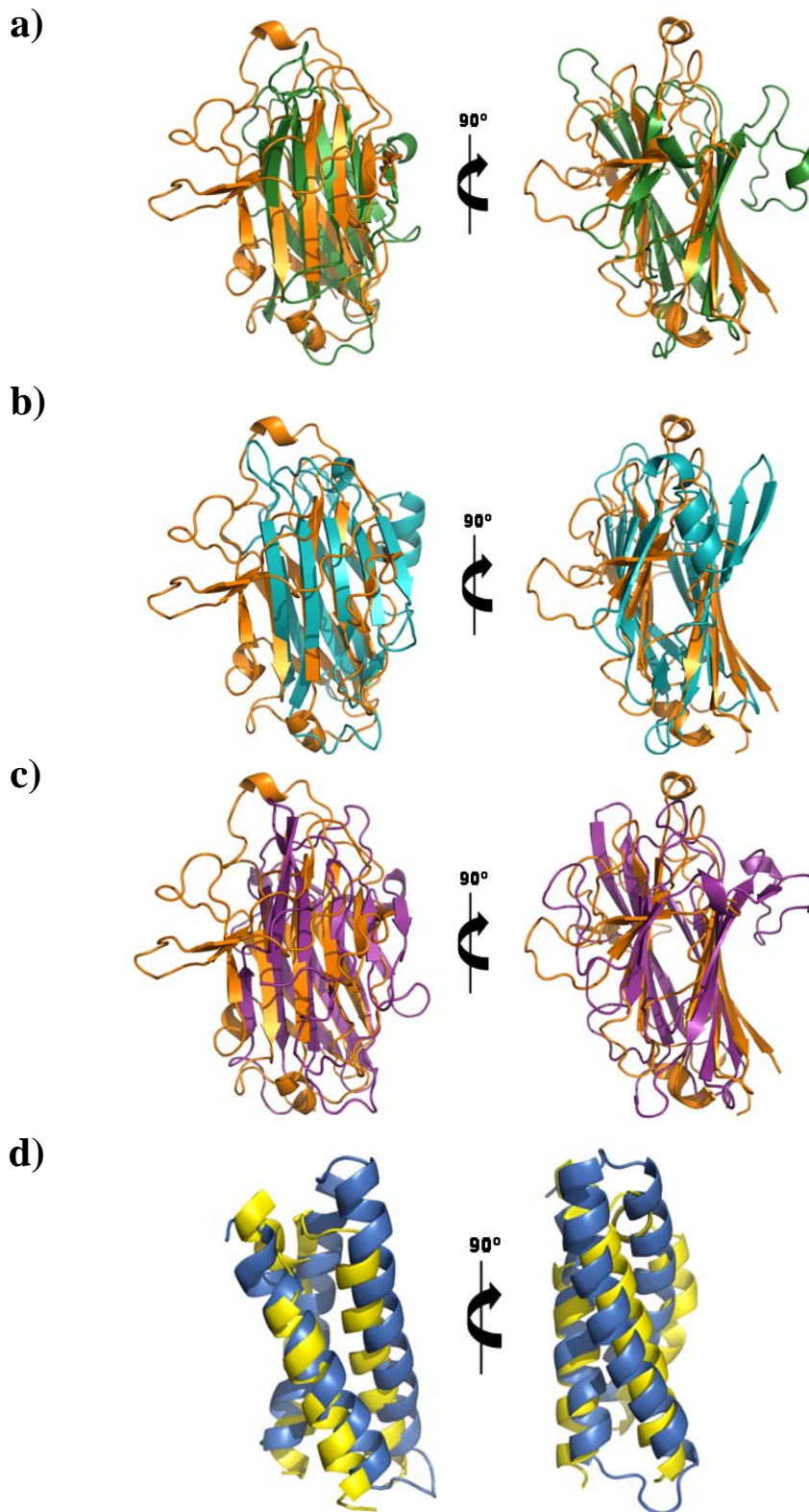


a)



b)

Supplementary Figure S8: a) Chemical shift perturbations of the observed H^N (top) and ^{15}N nuclei (bottom) in Fap1-NR α at 950 MHz. Differences between pH 8 and pH 6 are shown in black bars and between pH 8 and pH 5 in grey bars. Bar are absent if the resonance was not assigned. Acidic residues in the sequence are annotated in orange while the other residues significantly affected are highlighted in red. The secondary structure of the helical bundle is shown above. B) Ribbon representation of the NMR structure of Fap1-NR α at pH 8. As reported in the histograms, side-chains of acidic residues are shown in orange. Residues displaying significant pH-induced chemical shift changes are indicated in red. K207 in the proximity of E158 and E204 is shown in green.



Supplementary Figure S9: Structural homologs of Fap1-NR_α and Fap1-NR_β
 Superposition of Fap1-NR_β (orange) on the ligand-binding MSCRAMM domains of (a) fibrinogen-binding protein SdrG from *S. epidermidis* (pdb:1r17; chain A residues 433-581; green) (31,44), (b) the collagen binding protein ACE from *Enterococcus faecalis* (pdb:2z1p; chain A residues 174-316; teal) (45,46) and (c) the fibrinogen-binding protein clumping factor A from *Staphylococcus aureus* (pdb:1n67; chain A residues 378-560; purple) (48,49). Fap1-NR_β is shown in the same orientations as Fig. 2A. (e) Superposition of Fap1-NR_α (blue) on the giant, extracellular matrix-binding protein of staphylococci, EBH (pdb:2dgi; chain A residues 2-76; yellow) (50). Fap1-NR_α is shown in the same orientations as Fig. 2C.

Structural insights into serine-rich fimbriae from gram-positive bacteria

Stephanie Ramboarina, James A. Garnett, Meixian Zhou, Yuebin Li, Zhixiang Peng, Jonathan D. Taylor, Wei-chao Lee, Andrew Bodey, James W. Murray, Yilmaz Alguel, Julien Bergeron, Benjamin Bardiaux, Elizabeth Sawyer, Rivka Isaacson, Camille Tagliaferri, Ernesto Cota, Michael Nilges, Peter Simpson, Teresa Ruiz, Hui Wu and Stephen Matthews

J. Biol. Chem. published online June 28, 2010

Access the most updated version of this article at doi: [10.1074/jbc.M110.128165](https://doi.org/10.1074/jbc.M110.128165)

Alerts:

- [When this article is cited](#)
- [When a correction for this article is posted](#)

[Click here](#) to choose from all of JBC's e-mail alerts

Supplemental material:

<http://www.jbc.org/content/suppl/2010/06/28/M110.128165.DC1>

This article cites 0 references, 0 of which can be accessed free at <http://www.jbc.org/content/early/2010/06/28/jbc.M110.128165.full.html#ref-list-1>